

Self-Assembly

Cadmium(II)–Triazole Framework as a Luminescent Probe for Ca^{2+} and Cyano ComplexesYing Wang,^[a, c] Ping Xu,^[a] Qiong Xie,^[a] Qing-Qing Ma,^[a] Yan-Hui Meng,^[a] Zi-Wen Wang,^[a] Shaowei Zhang,^{*,[b, c]} Xiao-Jun Zhao,^{*,[a]} Jun Chen,^{*,[c]} and Zhong-Liang Wang^{*,[d]}

Abstract: A bidentate ligand, 1-[4-[4-(1*H*-1,2,4-triazol-1-yl)-phenoxy]phenyl]-1*H*-1,2,4-triazole (TPPT), has been designed and synthesized. By using TPPT as a building block for self-assembly with $\text{Cd}(\text{NO}_3)_2 \cdot 4\text{H}_2\text{O}$ and $\text{CdCl}_2 \cdot 10.5\text{H}_2\text{O}$, novel 1D double-chain $\{[\text{Cd}(\text{TPPT})(\text{NO}_3)_2] \cdot 3\text{H}_2\text{O}\}_n$ (**1**) and 2D (4,4) layer $[\text{Cd}(\text{TPPT})\text{Cl}_2(\text{H}_2\text{O})]_n$ (**2**) have been constructed. When **1** was employed as a precursor and exposed to DMF or *N,N'*-dimethylacetamide (DMAC), the crystals of **1** dissolved and reassembled into two types of brown block-shaped crystals of 1D double chains: $\{[\text{Cd}(\text{TPPT})_2(\text{NO}_3)_2] \cdot \text{DMF}\}_n$ (**1a**) and $\{[\text{Cd}(\text{TPPT})_2(\text{NO}_3)_2] \cdot \text{DMAC}\}_n$ (**1b**). The anion-exchange reac-

tions of complex **2** have also been investigated. After gently stirring crystals of **2** in $\text{CHCl}_3/\text{C}_2\text{H}_5\text{OH}/\text{H}_2\text{O}$ containing NaBr, $\text{NaI} \cdot 2\text{H}_2\text{O}$, or $\text{NaOAc} \cdot 3\text{H}_2\text{O}$, the crystals retained their crystalline appearances. A remarkable single crystal to single crystal transformation was observed and 1D double chains of $\{[\text{Cd}(\text{TPPT})\text{Br}_2] \cdot \text{C}_2\text{H}_5\text{OH}\}_n$ (**2a**) and $\{[\text{Cd}(\text{TPPT})_2] \cdot \text{CHCl}_3\}_n$ (**2b**), and 1D single chains of $[\text{Cd}(\text{TPPT})(\text{H}_2\text{O})_2(\text{CH}_3\text{COO})_2]_n$ (**2c**), can be obtained. Luminescent properties indicate that **1** shows excellent selectivity for Ca^{2+} and cyano complexes. To the best of our knowledge, this is the first example of a luminescent probe for Ca^{2+} based on triazole derivatives.

Introduction

Metal–organic frameworks (MOFs), a class of emerging porous materials, are built from metal ions/clusters connected by organic building blocks, in which the pore structures and functionalities are designable and predictable.^[1–3] Because there are numerous organic and inorganic functional moieties incorporated into the porous materials, MOFs demonstrate remarkable properties for applications in many fields, such as luminescence, gas storage, sensing, magnetics, and catalysis.^[4–7] Nowa-

days, porous metal–organic frameworks (PMOFs) with dynamic behavior have received considerable interest because these functional coordination frameworks can exhibit guest-induced structural changes of the host lattice.^[8] These porous frameworks contain potential or strain energy and undergo dramatic changes in functional properties and structure with the release of energy in response to specific external stimuli.^[9,10] An appropriate external stimulus can perturb the coordination sites of porous frameworks and its connectivity by inducing the breaking and generation of coordination bonds.^[11] Such a specific system can offer researchers an experimentally unexplored field to investigate and expand the subtle intermediate region between flexibility and robustness through dynamic single-crystal to single-crystal (SC–SC) and/or solid transformation processes, involving cooperative movements of atoms in the solid state, which has attracted considerable attentions in recent years.^[12] The SC–SC transformation is extremely desirable and useful, although it occurs relatively rarely, because it allows unequivocal assignment of the obtained product.^[13] Recent research in our group has mainly focused on the study of anion- or solvent-exchange properties and organic-group-functionalized aromatic guest loaded host–guest complex.^[14] Along this line, many researchers are interested in developing novel metal-based guest receptors that can function efficiently and selectively in aqueous or organic solvent environments.

Recently, significant progress has been made in the use of the luminescence properties of MOFs for the sensing of small molecules,^[15] metal ions,^[16] and explosives.^[17] Generally, diverse pore topologies and functional sites make MOFs suitable sensory materials through molecular-level interactions between the framework and the analytes.^[16g] An efficient strategy to

[a] Prof. Y. Wang, P. Xu, Q. Xie, Q.-Q. Ma, Y.-H. Meng, Dr. Z.-W. Wang, Prof. Dr. X.-J. Zhao
Key Laboratory of Inorganic–Organic
Hybrid Functional Material Chemistry, Ministry of Education
College of Chemistry, Tianjin Normal University, Tianjin 300387 (P.R. China)
E-mail: hxyzyxj@mail.tjnu.edu.cn

[b] Dr. S. Zhang
Key Laboratory of Theoretical Organic Chemistry
and Functional Molecule of the Ministry of Education
School of Chemistry and Chemical Engineering
Hunan University of Science and Technology, Xiangtan 411201 (P.R. China)
E-mail: swzhang@hnust.edu.cn

[c] Prof. Y. Wang, Dr. S. Zhang, Prof. Dr. J. Chen
Key Laboratory of Advanced Energy Materials Chemistry
Ministry of Education, Nankai University, Tianjin 300071 (P.R. China)
E-mail: chenabc@nankai.edu.cn

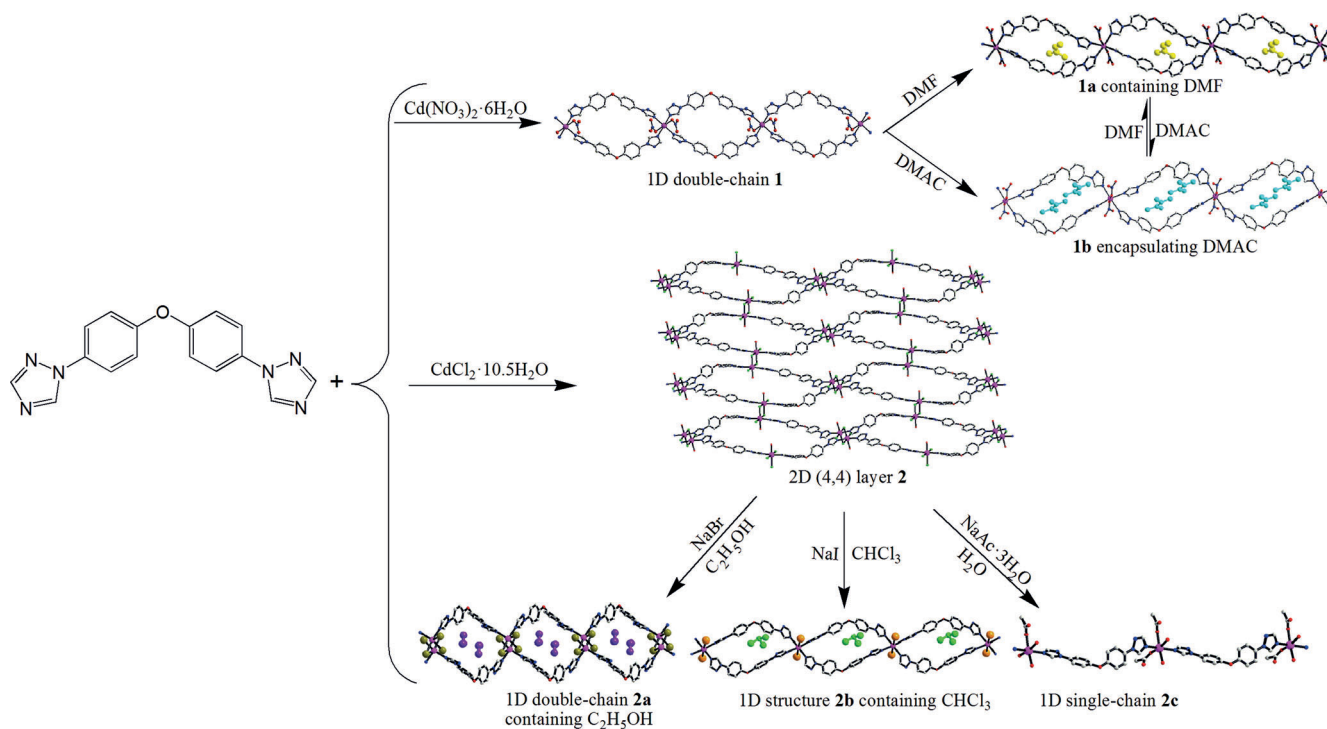
[d] Prof. Dr. Z.-L. Wang
Tianjin Key Laboratory of Water Resources and Environment Tianjin Normal
University, Tianjin 300387 (P.R. China)
E-mail: wangying790601@163.com
zhongliang_wang@163.com

Supporting information for this article is available on the WWW under
<http://dx.doi.org/10.1002/chem.201600209>.

prepare MOFs for the use in metal-ion sensing is to use aromatic organic molecules with nonbonded functional ligand sites, in which the aromatic part provides luminescence, and the nonbonded functional sites interact with the metal ions.^[18] However, immobilization of functional sites within the MOFs is still challenging due to their high reactivity during the synthesis of MOFs.^[16n]

However, the design and synthesis of such materials is still a tremendous challenge for researchers because of many factors, such as reaction temperature, solvent, anion, and molar ratio, although much progress has been made in practical and theoretic approaches. Among the strategies used, judiciously choosing a suitable polydentate organic ligand to construct the desirable product for self-assembly between metal ions and ligands has been receiving increasing attention.^[19] Generally, the preparation of such materials can be influenced by a number of factors, such as crystallization conditions, ligand/metal ratio, reaction systems of different solvents, and the nature of organic linkers. Particularly, the organic building blocks play an important role in the construction of MOFs with versatile structures. It is widely known that five-membered heterocycles, such as imidazole, pyrazole, triazole, and tetrazole, are good candidates in the design and synthesis of functional MOFs. Among them, 1,2,4-triazole and its derivatives have attracted great interest as multidentate ligands, which can bridge different metal centers to construct many novel coordination functional frameworks because of their versatile bridging features.^[20] On the basis of the above considerations, herein, we describe the design and synthesis of a new bidentate ligand, 1-{4-[4-(1*H*-1,2,4-triazol-1-yl)phenoxy]phenyl}-1*H*-1,2,4-triazole (TPPT). To the best of our knowledge, the flexible

ligand TPPT with L^2 symmetry has never been reported in coordination chemistry up to now. The continuous development of new ligand systems is important for the development of MOF chemistry. By using the phenoxy-based ligand TPPT, two Cd^{II} complexes, {[Cd(TPPT)(NO₃)₂] \cdot 3 H₂O}_n (**1**) and [Cd(TPPT)Cl₂(H₂O)]_n (**2**), have been constructed (Scheme 1). When **1** was employed as a precursor and exposed to DMF or DMAC, through our careful observation, the crystals of **1** were dissolved and reassembled into two types of yellow crystals: {[Cd(TPPT)₂(NO₃)₂] \cdot DMF}_n (**1a**) and {[Cd(TPPT)₂(NO₃)₂] \cdot DMAC}_n (**1b**; Scheme 1). We also investigated the anion-exchange reactions of complex **2**. After gently stirring crystals of **2** in a mixture of CHCl₃/C₂H₅OH/H₂O containing NaBr, NaI \cdot 2 H₂O, and NaOAc \cdot 3 H₂O, the crystals retained their crystalline appearances. A remarkable SC–SC transformation was observed and two 1D double chains of {[Cd(TPPT)Br₂] \cdot CH₃CH₂OH}_n (**2a**), and {[Cd(TPPT)₂] \cdot CHCl₃}_n (**2b**), and a 1D single chain of [Cd(TPPT)(H₂O)₂(CH₃COO)₂]_n (**2c**; Scheme 1), could be obtained. Luminescent properties indicate that **1** shows excellent selectivity for Ca²⁺. Complexes **1**, **2**, and **2c** exhibit strong ligand-originated photoluminescence emissions, which are selectively sensitive to electron-deficient nitroaromatic explosives, such as nitrobenzene (NB), 1,4-dinitrobenzene (*p*-DNB), 1,3-dinitrobenzene (*m*-DNB), and 1-fluoro-4-nitrobenzene (FNB). These properties make complexes **1**, **2**, and **2c** potential fluorescence sensors for these chemicals. Furthermore, complex **2** can detect cyano complexes, such as K₃[Cr(CN)₆], K₄[W(CN)₈], K₃[Mn(CN)₆], Na₃[W(CN)₈], Na₃[Mo(CN)₈], Cs₃[W(CN)₈], [NBu₃][Mo(CN)₈], [NBu₃][W(CN)₈], and Rb₃[W(CN)₈]. To the best of our knowledge, this is the first report on the application of MOFs for the sensing of cyano complexes.



Scheme 1. Synthesis of complexes **1**, **1a**, **1b**, **2a**, **2b**, and **2c**.

Results and Discussion

Structural descriptions of TPPT

TPPT crystallizes in the monoclinic crystal system with space group $P21/c$. The fundamental structural unit of TPPT is shown in Figure 1. The dihedral angles between the triazole and benzene rings are 10.2 and 1.9°, respectively, while the dihedral angle between the two benzene rings is 66°. Crystallographic data, selected bond lengths, and bond angles of TPPT are listed in Tables S1 and S2.

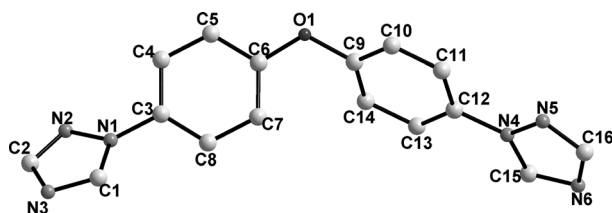


Figure 1. The fundamental structural unit of TPPT. Light gray, C; medium gray, N; dark gray, O.

Structural descriptions of complex 1

Complex 1 crystallizes in the triclinic crystal system with space group $P\bar{1}$ (Table 1). As shown in Figure 2, the fundamental structural unit of 1 contains one crystallographically independent Cd^{II} ion, one TPPT ligand, two terminally coordinated NO₃⁻ anions, and three crystal lattice water molecules. Each Cd^{II} center lies on a crystallographic inversion center and adopts a slightly distorted octahedral {CdN₄O₂} environment, involving four N atoms from four TPPT ligands and two O atoms from two monodentate nitrate.

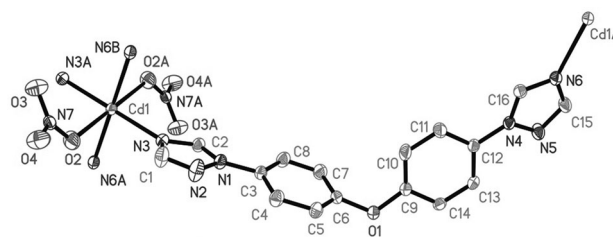


Figure 2. The fundamental structural unit of 1.

The Cd–N bond lengths are 2.326(3) and 2.361(1) Å (Table 2), respectively, whereas the axial Cd–O distance is 2.344(3) Å, which is shorter than that of Cd–O (2.373 Å) in [Cd₂(μ₂-L¹)₃(L¹)₂(NO₃)(μ₂-NO₃)(H₂O)₂](NO₃)₂·1.75 H₂O (L¹ = 4-(pyridin-2-yl)-1,2,4-triazole)^[21] and Cd–O (2.3563(18) Å) in Cd(L)₂(NO₃)₂·2 (THF) (L = 3,5-bis[3-pyridyl-3-(3'-methylphenyl)-1,3,4-oxadiazole]).^[22] The Cd^{II} nodes are connected to each other to form an infinite 1D chain that consists of a 32-membered bimetallic macrocycle-containing building block (Figure S1 a), in which the terminal triazole groups on each *cis*-TPPT ligand are basically perpendicular to each other. The dihedral angle between the triazole and benzene rings is 10.2 and 19.4°, respectively, much less than that of two terminal triazole groups (78.6°).

In each elliptical ring, the Cd...Cd contact is around 16 Å, whereas the opposite phenoxy O...O distance is around 10 Å. These 1D macrocycle-containing double chains (Figure 3) stack together in an –AA– fashion along the crystallographic *a* axis to generate distorted quadrangle-like channels (Figure S1b), in which the coordinated NO₃⁻ anions and water guest molecules are located; this is further confirmed by thermogravimetric analysis (TGA). TGA revealed that the encapsulated water molecules could be completely removed at temperatures ranging

Table 1. Crystallographic data and details of refinements for complexes 1, 1 a, 1 b, 2, 2 a, 2 b, and 2 c.^[a,b]

	1	1 a	1 b	2	2 a	2 b	2 c
formula	C ₃₂ H ₃₀ CdN ₁₄ O ₁₁	C ₃₅ H ₃₁ CdN ₁₅ O ₉	C ₃₆ H ₃₃ CdN ₁₅ O ₉	C ₁₆ H ₁₈ CdCl ₂ N ₆ O ₃	C ₁₈ H ₁₈ Br ₂ CdN ₆ O ₂	C ₃₃ H ₂₅ CdCl ₃ I ₂ N ₁₂ O ₂	C ₂₀ H ₂₂ CdN ₆ O ₇
<i>M_r</i> [g mol ⁻¹]	899.10	918.15	932.17	525.66	622.60	1094.20	570.84
crystal system	triclinic	triclinic	triclinic	triclinic	triclinic	triclinic	monoclinic
space group	<i>P</i> $\bar{1}$	<i>P</i> $\bar{1}$	<i>P</i> $\bar{1}$	<i>P</i> $\bar{1}$	<i>P</i> $\bar{1}$	<i>P</i> $\bar{1}$	<i>P</i> 21/ <i>c</i>
<i>T</i> [K]	296(2)	173(2)	173(2)	173(2)	296(2)	296(2)	296(2)
<i>a</i> [Å]	8.0811(9)	7.8147(10)	7.8957(5)	7.6240(6)	7.8782(9)	8.2403(4)	13.4303(19)
<i>b</i> [Å]	10.6838(10)	12.3663(16)	12.4931(8)	11.5346(9)	11.9129(13)	12.4512(6)	10.7261(15)
<i>c</i> [Å]	12.4221(13)	19.775(2)	19.8295(12)	12.6334(10)	12.6519(15)	19.8409(10)	16.355(2)
α [°]	110.930(2)	82.610(2)	82.1260(10)	104.2300(10)	103.229(2)	82.8880(10)	90
β [°]	105.489(2)	82.357(2)	83.0880(10)	106.0110(10)	107.760(2)	84.2980(10)	104.988(2)
γ [°]	98.246(2)	73.666(2)	75.4730(10)	103.4370(10)	104.294(2)	72.6360(10)	90
<i>V</i> [Å ³]	930.74(17)	1809.2(4)	1868.1(2)	979.92(13)	1034.6(2)	1923.80(16)	2275.8(6)
<i>Z</i>	1	2	2	2	2	2	4
<i>F</i> (000)	456	932	948	524	604	1056	1152
ρ_{calcd} [mg m ⁻³]	1.604	1.685	1.657	1.782	1.999	1.889	1.666
μ [mm ⁻¹]	0.666	0.684	0.664	1.418	4.945	2.429	1.014
data/restraints/parameters	3283/0/250	6368/88/561	6583/0/553	3423/0/235	3627/42/276	6723/60/491	4011/0/309
GOF on <i>F</i> ²	1.006	1.051	1.040	1.083	1.050	1.050	1.049
<i>R</i> ₁ ^[a] (<i>I</i> = 2 σ (<i>I</i>))	0.0346	0.0706	0.0318	0.0194	0.0458	0.0364	0.0210
ωR ₂ ^[b] (all data)	0.0753	0.1775	0.0690	0.0509	0.1254	0.1009	0.0586

[a] $R_1 = \sum (|F_o| - |F_c|) / \sum |F_o|$. [b] $\omega R_2 = [\sum w(|F_o|^2 - |F_c|^2)^2 / w |F_o|^2]^{1/2}$.

Table 2. Selected bond lengths [Å] and angles [°] for complexes **1**, **1 a**, **1 b**, **2 a**, **2 b**, and **2 c**.^[a]

1					
Cd1–N3	2.326(2)	Cd1–O2#1	2.344(2)	Cd1–N6#2	2.361(2)
N3–Cd1–N3#1	180.00(12)	N3–Cd1–O2#1	97.45(8)	N3#1–Cd1–O2#1	82.55(8)
N3#1–Cd1–O2	97.45(8)	O2#1–Cd1–O2	180.0	N3–Cd1–N6#2	85.78(7)
N3#1–Cd1–N6#2	94.22(7)	O2#1–Cd1–N6#2	81.35(8)	O2–Cd1–N6#2	98.65(8)
1 a					
Cd1–O6	2.259(6)	Cd1–N12#1	2.302(5)	Cd1–N3	2.326(5)
Cd1–N9	2.334(5)	Cd1–O3	2.349(5)	Cd1–N6#1	2.363(5)
O6–Cd1–N12#1	83.1(2)	O6–Cd1–N3	99.8(2)	N12#1–Cd1–N3	171.44(17)
O6–Cd1–N9	85.44(19)	N12#1–Cd1–N9	96.49(17)	N3–Cd1–N9	91.79(17)
O6–Cd1–O3	177.70(19)	N3–Cd1–O3	81.06(18)	N12#1–Cd1–O3	96.34(18)
N12#1–Cd1–N6#1	81.94(19)	N9–Cd1–O3	92.40(16)	N3–Cd1–N6#1	89.57(18)
O6–Cd1–N6#1	101.8(2)	O3–Cd1–N6#1	80.29(18)	N9–Cd1–N6#1	172.27(17)
1 b					
Cd1–N9	2.312(2)	Cd1–N12#1	2.318(2)	Cd1–O6	2.359(2)
Cd1–O4	2.3316(19)	N3–Cd1–N12#1	171.59(7)	N9–Cd1–O4	97.60(7)
N9–Cd1–N3	93.48(7)	N3–Cd1–O4	82.69(7)	N12#1–Cd1–O4	99.31(7)
N9–Cd1–N12#1	94.35(7)	O4–Cd1–N6#1	80.87(7)	N12#1–Cd1–O6	79.92(8)
N9–Cd1–O6	83.55(7)	N9–Cd1–N6#1	176.42(8)	O4–Cd1–O6	178.67(8)
O6–Cd1–N6#1	97.93(7)	N12#1–Cd1–N6#1	82.74(7)	N3–Cd1–O6	97.92(7)
N3–Cd1–N6#1	89.55(7)				
2					
Cd1–N3	2.2970(18)	Cd1–N6#1	2.314(2)	Cd1–Cl2#2	2.5935(5)
Cd1–Cl1	2.6119(6)	Cd1–Cl1#3	2.6939(6)	Cd1–Cl2	2.8322(6)
N3–Cd1–N6#1	103.42(7)	N3–Cd1–Cl2#2	87.90(5)	N6#1–Cd1–Cl2#2	155.55(5)
N3–Cd1–Cl1	163.55(5)	N6#1–Cd1–Cl1	86.43(5)	Cl2#2–Cd1–Cl1	88.181(19)
N3–Cd1–Cl1#3	83.36(5)	N6#1–Cd1–Cl1#3	88.79(5)	Cl2#2–Cd1–Cl1#3	114.287(19)
Cl1–Cd1–Cl1#3	83.710(18)	N3–Cd1–Cl2	86.55(5)	N6#1–Cd1–Cl2	81.50(5)
Cl2#2–Cd1–Cl2	77.589(19)	Cl1–Cd1–Cl2	108.171(17)	Cl1#3–Cd1–Cl2	164.003(18)
2 a					
Br1–Cd1#1	2.7329(5)	Br1–Cd1	2.9970(6)	Br2–Cd1	2.7523(6)
Br2–Cd1#2	2.8181(6)	Cd1–N6#3	2.316(4)	Cd1–N3	2.335(3)
Cd1–Br1#1	2.7329(5)	Cd1–Br2#2	2.8181(6)	Cd1#1–Br1–Cd1	101.765(18)
Cd1–Br2–Cd1#2	95.149(17)	N6#3–Cd1–N3	98.92(13)	N6#3–Cd1–Br1#1	87.99(7)
N3–Cd1–Br1#1	160.09(10)	N6#3–Cd1–Br2	167.22(10)	N3–Cd1–Br2	87.89(10)
Br1#1–Cd1–Br2	89.150(16)	N6#3–Cd1–Br2#2	84.24(10)	N3–Cd1–Br2#2	90.98(10)
Br1#1–Cd1–Br2#2	108.359(19)	Br2–Cd1–Br2#2	84.850(17)	N6#3–Cd1–Br1	86.96(10)
N3–Cd1–Br1	83.48(10)	Br2–Cd1–Br1	104.640(17)	Br2#2–Cd1–Br1	168.758(16)
2 b					
Cd2–N12#1	2.380(4)	Cd2–N9	2.385(4)	Cd2–N3	2.409(4)
Cd2–N6#2	2.423(4)	Cd2–I1	2.9174(5)	Cd2–I2	2.9400(5)
N12#1–Cd2–N9	95.16(15)	N12#1–Cd2–N3	90.06(14)	N9–Cd2–N3	173.63(15)
N12#1–Cd2–N6#2	179.34(14)	N9–Cd2–N6#2	84.55(16)	N3–Cd2–N6#2	90.26(15)
N12#1–Cd2–I1	88.39(10)	N9–Cd2–I1	92.64(11)	N3–Cd2–I1	91.15(10)
N6#2–Cd2–I1	91.03(11)	N12#1–Cd2–I2	89.41(10)	N9–Cd2–I2	89.89(11)
N3–Cd2–I2	86.51(10)	N6#2–Cd2–I2	91.18(11)	I1–Cd2–I2	176.789(15)
2 c					
Cd1–O4	2.2550(16)	Cd1–O6	2.3137(16)	Cd1–N6#1	2.3331(18)
Cd1–N3	2.3333(19)	Cd1–O2	2.3355(15)	Cd1–O7	2.3641(17)
O4–Cd1–O6	103.31(6)	O4–Cd1–N6#1	98.75(7)	O6–Cd1–N6#1	87.39(7)
O4–Cd1–N3	95.36(7)	O6–Cd1–N3	84.13(7)	N6#1–Cd1–N3	164.89(7)
O4–Cd1–O2	82.32(6)	O6–Cd1–O2	173.99(6)	N6#1–Cd1–O2	93.90(6)
N3–Cd1–O2	93.30(6)	O4–Cd1–O7	169.35(6)	O6–Cd1–O7	87.32(6)
N6#1–Cd1–O7	80.78(7)	N3–Cd1–O7	86.35(7)	O2–Cd1–O7	87.09(6)

[a] Symmetry transformations used to generate equivalent atoms: for **1**: #1 $-x+2, -y, -z-1$ #2 $-x+1, -y, -z$ #3 $x+1, y, z-1$ #4 $x-1, y, z+1$; for **1 a**: #1 $x-1, y-1, z$ #2 $x+1, y+1, z$; for **1 b**: #1 $x+1, y+1, z$ #2 $x-1, y-1, z$; for **2**: #1 $x+2, y, z+1$ #2 $-x+2, -y, -z+2$ #3 $-x+3, -y, -z+2$ #4 $x-2, y, z-1$; for **2 a**: #1 $-x-1, -y+1, -z$ #2 $-x, -y+1, -z$ #3 $x-2, y, z-1$ #4 $x+2, y, z+1$; for **2 b**: #1 $x+1, y+1, z$ #2 $x-1, y-1, z$; for **2 c**: #1 $x-1, y, z-1$ #2 $x+1, y, z+1$.

from 200 to 220 °C (calculated 6.00%, observed 5.81%; Figure 4a). The powder X-ray diffraction (PXRD) patterns (Fig-

ure 4b) based on the desolvated sample of **1** confirm that the framework of **1** is stable.

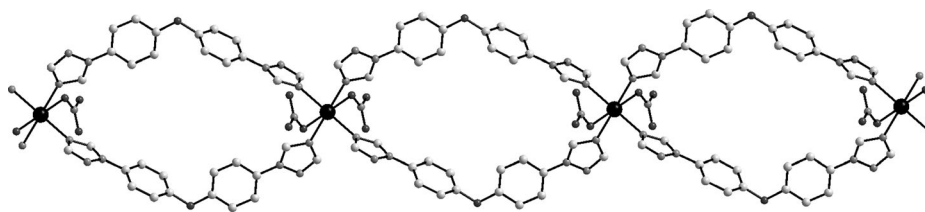


Figure 3. The 1D double-chain structure of **1** along the a axis. Black, Cd; light gray, C; medium gray, N; dark gray, O.

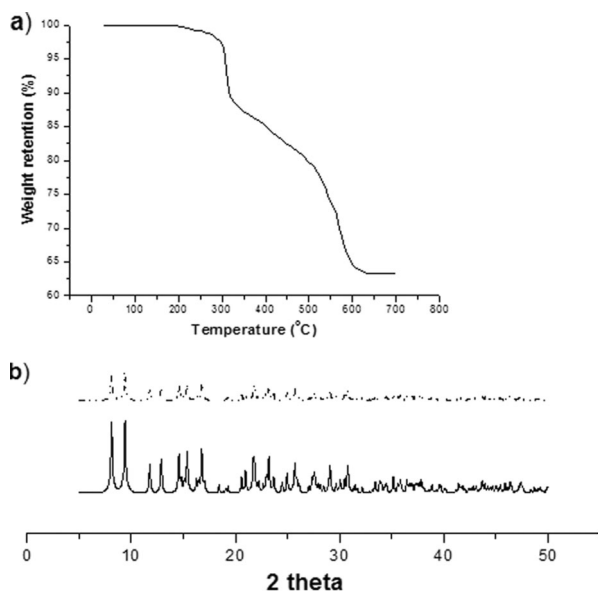


Figure 4. a) TGA trace of **1**. The calculated and observed weight losses corresponding to three encapsulated crystal lattice water molecules are 6.00 and 5.81%, respectively. b) PXRD patterns of **1**. Black straight line, simulated; black dotted line, as-synthesized.

Structural descriptions of complex **2**

Complex **2** is characterized by X-ray single-crystal analysis and crystallizes in the monoclinic system, space group $P2_1/c$ (Table 1 <xtabr1). As depicted in Figure 5, Cd1 is six-coordinated by three chloride anions (Cl1, Cl2, and Cl2A), two nitrogen atoms from two TPPT ligands (N3 and N6B), and one coordinated aqua oxygen O2 atoms, forming slightly distorted octahedral coordination geometry. Every TPPT adopts μ_2 -bridging modes and the dihedral angles between the benzene ring and triazole moiety are 18.5 and 33.3°, respectively, which indicates a spatial distortion effect. Two μ_2 -bridging chloride anions connect two neighboring Cd^{II} ions to form a binuclear Cd^{II} cluster, in which the Cd...Cd separation is 3.849(3) Å.

Such binuclear Cd^{II} clusters, {Cd₂Cl₂}, act as secondary building blocks (SBUs) and can be further linked through four bridging TPPT ligands to form a 2D porous framework (Figure 6). Topologically, if each {Cd₂Cl₂} cluster is considered as a basic node of a simplified network, then the topology of **2** can be regarded as a four-connected node and μ_2 -TPPT tecton linker. The TGA trace indicated that the coordinated water molecule could be removed by heating from 100 to 150 °C (calcd: 3.42%, obsd: 3.79%; Figure 7a). The remarkable difference be-

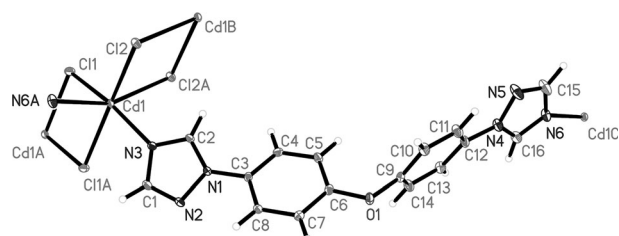


Figure 5. The fundamental structural unit of **2** (30% displacement ellipsoids for the non-hydrogen atoms).

tween **1** and **2** lies in the location of the anions. As mentioned above, the NO₃⁻ anions in **1** serving as terminal-coordinated ligands face toward the center of the channel, whereas the Cl⁻ anions in **2** act as bridging ligands to connect two neighboring Cd^{II} ions, forming a 2D four-connected network with (4,4) topology (Figure S2). Again, the PXRD pattern indicated that the as-synthesized complex **2** was pure (Figure 7b).

Molecular reassembly during the solvent-exchange process

In our previous work,^[14c] we employed mononuclear complex [Mn(tatr₂(SCN)₂(CH₃OH))·2H₂O] (tatr₂ = 1-[9-(1H-1,2,4-triazol-1-yl)anthracen-10-yl]-1H-1,2,4-triazole) to synthesize the reactive, organic-group-functionalized, aromatic-guest-loaded, host-guest 2D layer {[Mn(tatr₂(SCN)₂)]·(atan)}_n (atan = anthracene). After gently stirring the mononuclear Mn^{II} complex for 6 h, the complex dissolved and a remarkable reassembly process occurred. The mononuclear Mn^{II} complex was converted into the novel 2D coordination framework, encapsulating atan as an organic template. Encouraged by our results in reassembly, herein, we exposed the light-yellow crystals of complex **1** to DMF or DMAC for 6 h. We observed that crystals of **1** dissolved and reassembled into another two brown crystals of an isomorphous solvate of **1a** or **1b**. X-ray analysis revealed that the 1D chain families of **1a** and **1b** were supramolecular isomers, although they are topologically equivalent (Figures S3 and S4). On the other hand, the ¹³C and ¹H NMR spectra (Figures S5 and S6), together with TGA measurements (Figures S7 and S8) on the exchanged sample, demonstrated that the encapsulated water molecules were simultaneously replaced by DMF or DMAC molecules when the reaction was performed in DMF or DMAC. The structures of **1a** and **1b** are essentially isostructural to that of **1**, with similar cell dimensions and the same gross structural features (detailed bond parameters can be obtained from the archived CIF files). Single-crystal XRD analysis revealed

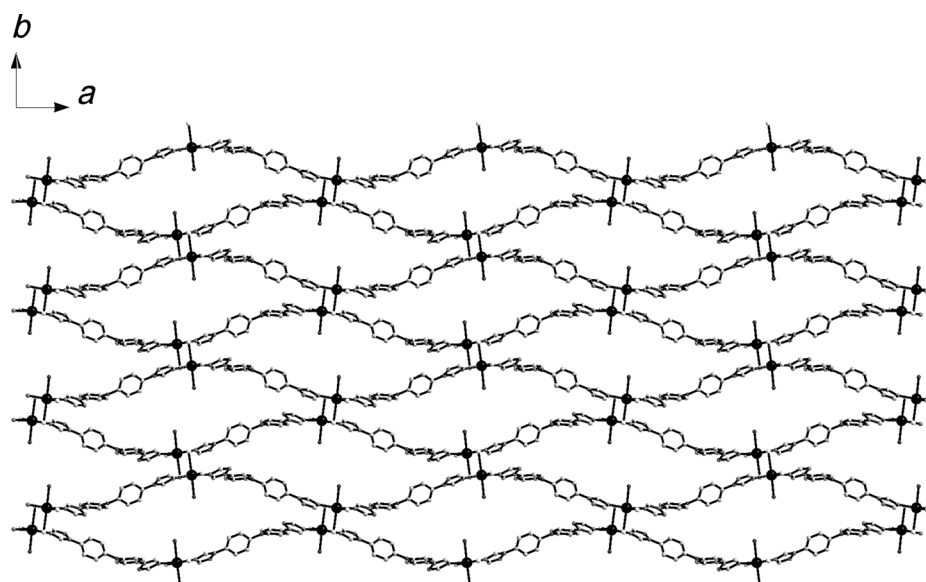


Figure 6. The 2D porous framework of **2** along the *c* axis. Black, Cd; light gray, C; medium gray, N; dark gray, O; white, Cl.

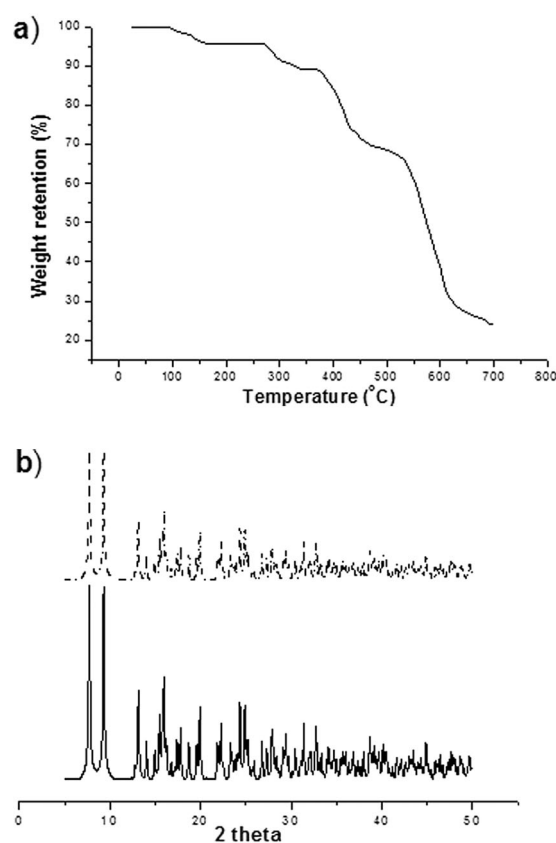


Figure 7. a) TGA trace of **2**. The calculated amount of coordinated H₂O for **2** is 3.42%, and the observed amount is 3.79%. b) PXRD patterns of **2**. Black straight line, simulated; black dotted line, as-synthesized.

that the Cd...Cd separations in **1a** and **1b** were 16.381 and 16.368 Å, respectively. The dihedral angles between benzene rings and triazole moieties are 23.5, 45.2, 19.9, and 2.3° in **1a** and 6.8, 43.4, 4.2, and 24.1° in **1b**. The flexible dihedral angles

reveal that the ligand TPPT can provide favorable conditions for the formation of Cd–N coordination bonds through the free torsion of C–N bonds.

Anion-exchange properties and transformation from a 2D layer to 1D double- or single-chain structures

The SC–SC structural transformations, which involve cooperative movements of atoms in the solid state, have received considerable attention in recent years.^[23] The SC–SC transformation is extremely useful and desirable, although it occurs relatively rarely, because it allows unequivocal assignment of the product obtained.^[13] Usually, through the SC–SC transformation, new complexes, which cannot be obtained under conventional conditions, can be formed in high yield.^[24] Materials that show reversible structure transformations and a characteristic response toward specific external stimuli, such as light,^[25] temperature,^[26] and guest molecules,^[27] are vitally important for applications in sensing, molecular capture, switches, and so on.^[28] However, studies on the changes in metal coordination geometry caused by the removal and addition of ligands from the network itself through the SC–SC transformation remain less common.^[29]

Generally, MOFs have low solubility and high stability in common solvents; therefore, these frameworks can retain their morphology through a solvent-assisted solid-state reaction, although in some examples the solid materials may lose their crystallinity. In recent years, previous research also demonstrated that solvent molecules could induce SC–SC transformations. In most examples, guest moieties of diverse shapes and sizes can be encapsulated in the MOFs cavities through various intermolecular interactions. Therefore, MOF products in such conversion processes exhibit a certain shape flexibility and size specificity, and have wide applications in many fields, such as selective molecular/ion recognition, separation, and molecular/

ion sensors.^[30] Although some related research in the construction of MOFs with framework structures by deliberately tuning different kinds of solvent molecules^[31,32] or different component ratios of mixed solvents^[33] have been reported, a particular series of MOF species that can be systematically tuned by the two factors in combination and also undergo structural transformations remain largely unexplored thus far. To further investigate the effect of solvent–molecule exchange on the SC–SC transformation, anion-induced crystal transformations, especially SC–SC transformations, have been widely investigated for coordination frameworks recently.^[14b,c,34] Herein, PXRD and well-defined single-crystal diffraction analysis methods were employed to monitor related dynamic conversions between some crystalline solids. Notably, for related dynamic conversions between other MOFs, the product cannot be definitely characterized by the available methods; thus they are not referred to herein. Recently, we obtained $\{[\text{Cu}(\text{tatr}_2)_2(\text{NO}_3)_2] \cdot (\text{CH}_3\text{OH}) \cdot 4\text{H}_2\text{O}\}_n$, in which NO_3^- anions could be completely exchanged by ClO_4^- in an irreversible SC–SC transformation, as evidenced by the anion-exchange products of $\{[\text{Cu}(\text{tatr}_2)_2(\text{H}_2\text{O})_2] (\text{ClO}_4)_2 \cdot 4\text{CH}_3\text{OH}\}_n$.^[14c] Taking inspiration from the aforementioned points,^[35] herein we investigated the anion-exchange reaction of the 2D architecture of **2**. After gently stirring crystals of **2** (0.5 mmol) in a 1:8:1 solution of $\text{CHCl}_3/\text{C}_2\text{H}_5\text{OH}/\text{H}_2\text{O}$ containing $\text{NaBr} \cdot 2\text{H}_2\text{O}$, $\text{NaI} \cdot 2\text{H}_2\text{O}$, or $\text{NaOAc} \cdot 3\text{H}_2\text{O}$ (5 mmol) for 6 h, the crystals retain their crystalline appearances, excluding dissolution or recrystallization processes. A remarkable anion- and solvent-exchange in a SC–SC transformation was observed and two 1D double chains of **2a** and **2b**, and a 1D single chain of **2c**, can be obtained.

Single-crystal XRD studies revealed that **2a** crystallized in the triclinic crystal system with space group $P\bar{1}$ (Table 1). In **2a**, Cd1 coordinates to two nitrogen atoms (N3 and N6) from two TPPT ligands and three bromide ions (Br1, Br2, and Br2A). The bond lengths of Cd–N and Cd–Br are 2.316(4)–2.335(3) and 2.7329(5)–2.9970(6) Å (Table 2), respectively. As demonstrated in Figure 8, the coordination environment of the Cd^{II} ion can be viewed as a distorted tetragonal pyramid.

Two μ_2 -Br⁻ connect two Cd^{II} ions to form the binuclear $\text{Cd}_2^{\text{II}}\text{Br}_4\text{N}_4$, which is extended into a 1D infinite chain through four μ_2 -TPPT ligands. Careful investigation shows that the intercalated $\text{C}_2\text{H}_5\text{OH}$ molecules and coordinated Br⁻ play key roles in differentiating between the two structures **2** and **2a**. The corresponding dihedral angles between the benzene rings and triazole moieties in **2a** are 10.8 and 22.3°, respectively. Interestingly, complex **2a** has larger 1D channels, with the

dimensions of 9.766(10) × 11.021(13) Å, than those of **1** (9.715 (9) × 9.822(11) Å), due to the larger size of encapsulated guest molecules of $\text{C}_2\text{H}_5\text{OH}$ than H_2O . TGA (Figure 9a) revealed that encapsulated $\text{C}_2\text{H}_5\text{OH}$ could be completely removed at temperatures ranging from 200 to 269 °C (calcd: 8.75 %, obsd: 8.64 %). The PRXD patterns (Figure 9b) based on the desolvated sample of **2a** confirm that the $[\text{Cd}(\text{TPPT})_2]$ framework is stable.

Single-crystal analysis revealed that complexes **2b** and **1** were isostructural (Figures S9 and S10). They all crystallized in the triclinic space group $P\bar{1}$ (Table 1). The $\text{Cd}^{\text{II}} \cdots \text{Cd}^{\text{II}}$ distance was about 16 Å and encapsulated CHCl_3 was located in the quadrangle channels with dimensions of 9.828(5) × 9.929(4) Å².

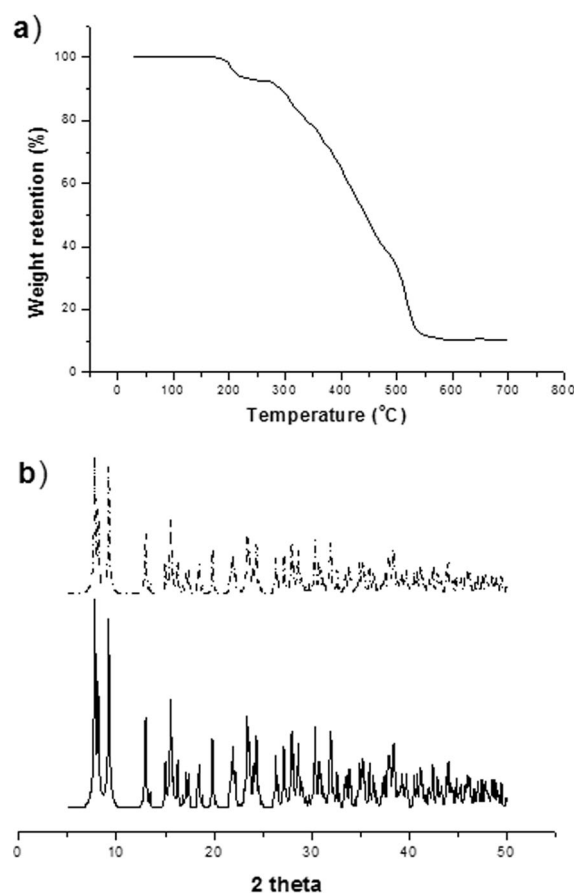


Figure 9. a) TGA trace of **2a**. The calculated amount of encapsulated $\text{C}_2\text{H}_5\text{OH}$ in $\{[\text{Cd}(\text{TPPT})\text{Br}_2] \cdot \text{C}_2\text{H}_5\text{OH}\}_n$ is 8.75 %, and the observed amount is 8.64 %. b) PXRD patterns of **2a**. Black straight line, simulated; black dotted line, as-synthesized.

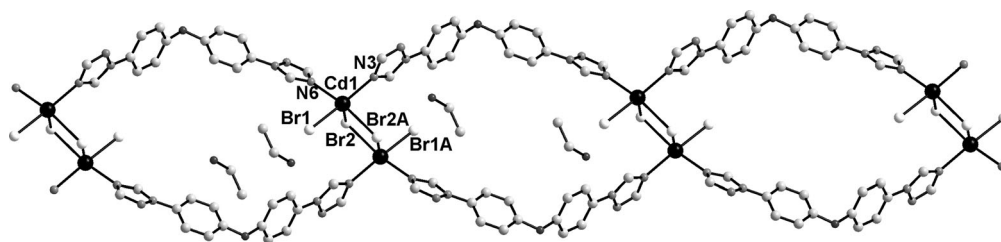


Figure 8. The 1D nanotubular structure of **2a** encapsulating guest water molecules. Black, Cd; white, Br; dark gray, O; light gray, C; medium gray, N.

The dihedral angles between benzene and triazole rings in **2b** are 5.0 and 40.3°, respectively. TGA (Figure S11a) revealed that encapsulated C₂H₅OH could be completely removed at temperatures ranging from 150 to 240 °C (calcd: 10.91 %, obsd: 10.90 %). The PRXD patterns based on the desolvated sample of **2b** confirmed that the 1D chain was stable (Figure S11b).

As shown in Figure 10, the asymmetric unit of **2c** contains one crystallographically independent Cd^{II} ion, one TPPT ligand, two terminally coordinated CH₃COO⁻ anions, and two terminally coordinated water molecules. The geometry of the Cd1 atom can be regarded as a distorted octahedron, which is coordinated by two triazole nitrogen atoms from two TPPT (N3 and N6A), two terminally coordinated CH₃COO⁻ anions (O2 and O4), and two terminally coordinated water molecules (O6 and O7). The Cd–N bond lengths are in the range of 2.333(1)–2.333(3) Å (Table 2), which are typical values for these bonds. As illustrated in Figure 11, each TPPT bridges two neighboring Cd^{II} ions to form the 1D single chain with a Cd...Cd distance of 18.282(23) Å. TGA (Figure 12a) revealed that the coordinated H₂O molecules could be completely removed at temperatures ranging from 150 to 250 °C (calcd: 3.15 %, obsd: 3.35 %). The PRXD patterns (Figure 12b) based on the desolvated sample of **2c** confirmed that the 1D single chain was stable.

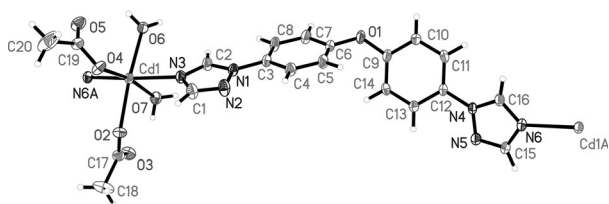


Figure 10. The fundamental structural unit of **2c** (30% displacement ellipsoids for the non-hydrogen atoms).

Luminescence behavior and sensing properties

Aromatic organic molecules and inorganic–organic hybrid coordination complexes were investigated for their photoluminescent properties and for potential applications as luminescent materials, such as light-emitting diodes (LEDs).^[36] Owing to the ability to adjust the emission strength and wavelength of organic materials, the construction of inorganic–organic coordination complexes through the judicious incorporation of transition-metal centers and conjugated organic spacers can be an efficient strategy to synthesize new kinds of photoluminescent materials. It is known that a double bond is composed of σ and π bonds, and the emissions of organic ligands are usually ascribed to $\pi^* \rightarrow n$ or $\pi \rightarrow \pi^*$ transitions.^[37] It is then ex-

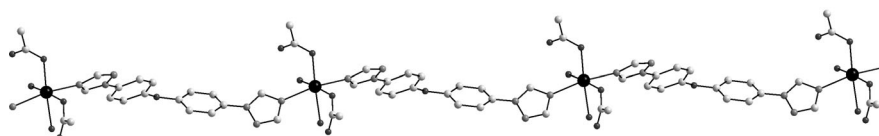


Figure 11. The infinite 1D single chain of **2c**. Black, Cd; dark gray, O; light gray, C; medium gray, N.

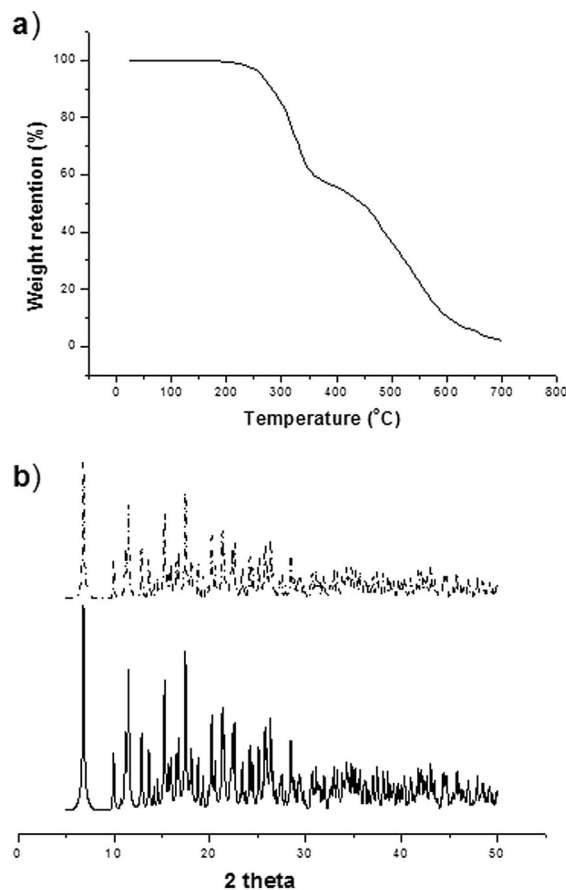


Figure 12. a) TGA trace of **2c**. The calculated amount of coordinated H₂O molecules in [Cd(TPPT)(H₂O)₂(CH₃COO)₂]_n is 3.15 %, and the observed amount is 3.35 %. b) PXRD patterns of **2c**. Black straight line, simulated; black dotted line, as-synthesized.

pected that the double-bond-based ligand TPPT will exhibit photoluminescence properties. Previous research also confirmed that coordination polymers had the ability to affect the emission strength and wavelength of organic materials through the judicious incorporation of different central metal ions.^[38] Herein, the luminescent properties of TPPT and complexes **1**, **1a**, **1b**, **2**, **2a**, **2b**, and **2c** in the solid state and in DMF have been investigated.

At ambient temperature, strong green fluorescence for TPPT and complexes **1**, **1a**, **1b**, **2**, **2a**, **2b**, and **2c** in the solid state is visible in daylight by irradiation with UV light. The emission spectra are shown in Figure 13; all of the complexes and TPPT were excited at $\lambda = (385 \pm 2)$ nm. The main emission bands of TPPT and complexes **1**, **1a**, **1b**, **2**, **2a**, **2b**, and **2c** are located at $\lambda = 525, 515, 511, 492, 487, 518, 526,$ and 546 nm, respec-

tively, exhibiting strong green fluorescence with a slightly different band shape. All complexes also exhibit some low-energy emission bands. The different band shapes in the luminescent emissions might be due to different structural topologies. The emissions of complexes **1**, **1a**, **1b**, **2**, **2a**, **2b**, and **2c** are neither metal-to-ligand charge transfer (MLCT) nor ligand-to-metal charge transfer (LMCT) in nature and can probably be assigned to intraligand fluorescent emission because very similar emissions are also observed for the free TPPT ligand. The enhancement of intraligand fluorescence in complexes **1**, **1a**, **1b**, **2**, **2a**, **2b**, and **2c** is probably due to the coordination of TPPT to Cd^{II}, which increases the conformational rigidity of the ligand, thereby reducing the nonradiative decay of the intraligand (π - π^*) excited state.^[39]

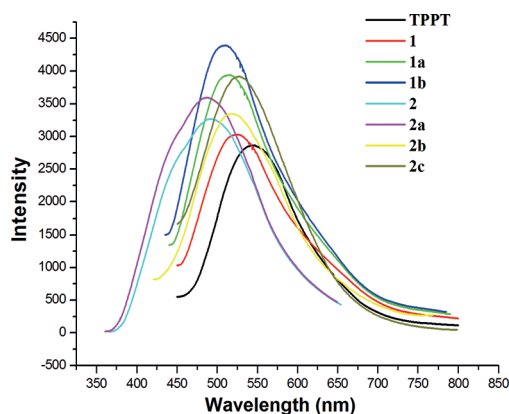


Figure 13. Emission spectra of TPPT, complexes **1**, **1a**, **1b**, **2**, **2a**, **2b**, and **2c** in the solid state at room temperature. All compounds were excited at $\lambda = (385 \pm 2)$ nm.

As displayed in Figure 14, TPPT and complexes **1**, **1a**, **1b**, **2**, **2a**, **2b**, and **2c** exhibit broad blue fluorescence in DMF. All of the complexes in DMF are excited at $\lambda = (365 \pm 5)$ nm. The main emission bands of the complexes are located at $\lambda = 540$, 434, 446, 438, 477, 508, 516, and 522 nm, respectively, exhibiting strong green fluorescence with slightly different band shapes. The fluorescent emissions can probably be assigned to intraligand fluorescent emission because similar behavior is also observed for the free TPPT ligand in DMF. Coordination of the complexes leads to slight redshifts of the emissions. Compared with the fluorescent emissions of **1**, **1a**, **1b**, **2**, **2a**, **2b**, and **2c** in solution, the emissions are redshifted and narrow; this can be attributed to intermolecular interactions in the solid state, most likely π - π^* stacking interactions.

In our previous studies, the selectivity and sensitivity to Mg²⁺, Cd²⁺, and Zn²⁺ were mainly investigated.^[14b,c] Inspired by the aforementioned progress in the study of luminescent probes based on triazole derivatives, herein, luminescent investigations reveal that **1** can detect Ca²⁺ ions with relatively high sensitivity and selectivity. The emission intensity of **1** significantly increases upon adding one to three equivalents of Ca²⁺ ions (from CaCl₂) with respect to **1** (Figure 15). The highest band at $\lambda = 434$ nm is about four times as intense as the corresponding band in DMF without Ca²⁺ ions. To further under-

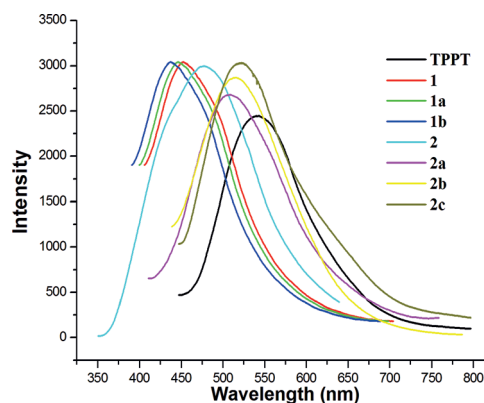


Figure 14. Emission spectra of TPPT and complexes **1**, **1a**, **1b**, **2**, **2a**, **2b**, and **2c** in DMF at room temperature (1×10^{-3} mol L⁻¹).

stand this experimental phenomenon, the same experiments were performed with the introduction of Mg²⁺ (MgCl₂), Ni²⁺ (NiCl₂), and Zn²⁺ (ZnCl₂) ions into the system. The results reveal that the luminescent intensities of **1** decrease. It is interesting that, upon adding Cd²⁺ (CdCl₂) or Co²⁺ (CoCl₂) ions, the emission intensity of **1** exhibits almost the same intensity as that of **1**. The above experimental results support the idea that the luminescent emission of **1** shows excellent selectivity for Ca²⁺. This is the first example of a 1D coordination complex based on triazole derivatives as a luminescent probe of Ca²⁺. However, when adding one to three equivalents of M²⁺ ions (M = Cd²⁺, Ca²⁺, Co²⁺, Mg²⁺, Ni²⁺, and Zn²⁺) with respect to **1a**, **1b**, and **2**, **2a**, **2b**, and **2c**, the luminescence bands are not enhanced, but rather decrease, as illustrated in Figures S12–S17.

In addition, we have examined the plausible modulation of its porous network by means of ion-exchange processes of the extra-framework cations. The results show that the ion-exchange processes in these systems lead to profound changes in the luminescent properties. The radii of Cd²⁺, Ca²⁺, Co²⁺, Mg²⁺, Ni²⁺, and Zn²⁺ are 95, 100, 90, 57, 72, 69, and 74 pm, respectively. Among these ions, perhaps the size of Cd²⁺ may coincide with the size of the cavity of the 1D double chain and increase the luminescent intensity of **1**.

With the development of modern society and industry, hazardous chemicals, such as toxic ions and organic small molecules, are increasingly released from industrial facilities and other anthropogenic activities; these have adverse effects on human health and the environment. Environmental pollutants, such as poisonous gases, organic solvent vapors, heavy metals, and anions, have both acute and chronic effects on human health and consequently lead to heart attacks, lung cancer, hepatitis, and other serious diseases.^[40] It is challenging and of great significance to identify and monitor these environmental pollutants through direct detection by the naked eye through the development of advanced materials. Considering the intense luminescent signal and visible luminescent colors, Cd MOFs could be good candidates as luminescent sensing materials for environmental pollutants. To explore the lumines-

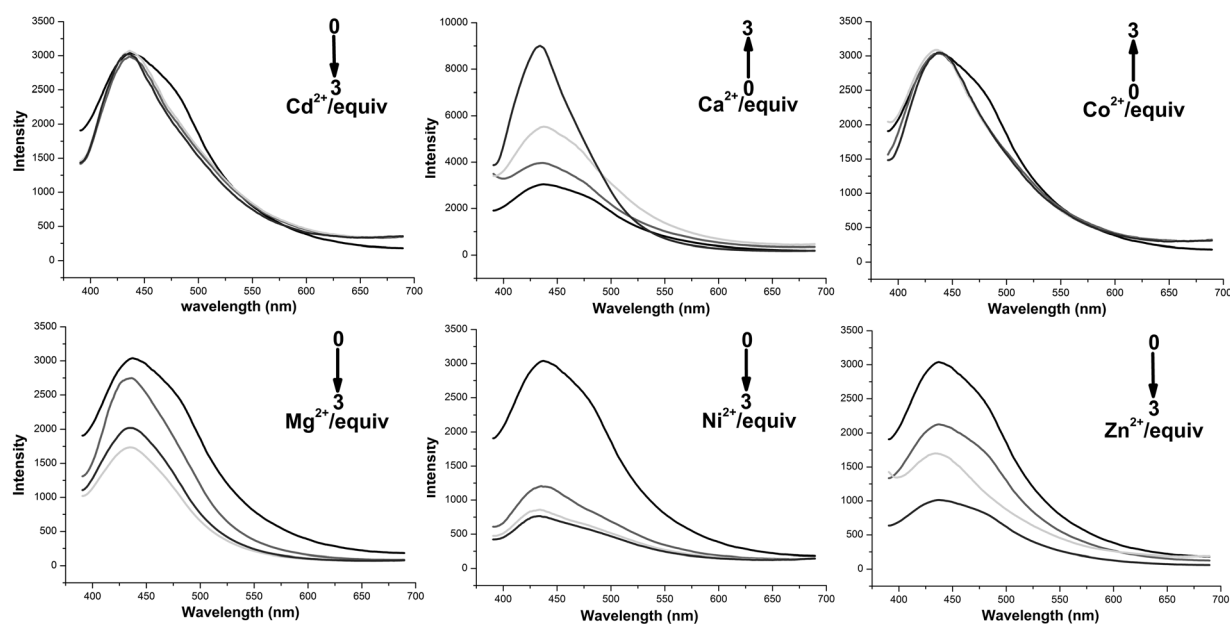


Figure 15. Emission spectra of complex **1** in DMF (10^{-3} M) at room temperature (excited at $\lambda = 400$ nm) in the presence of 0–3 equivalents of Cd^{2+} (top left), Ca^{2+} (top middle), Co^{2+} (top right), Mg^{2+} (bottom left), Ni^{2+} (bottom middle), and Zn^{2+} (bottom right).

cent properties of Cd MOFs in sensing, luminescent Cd^{2+} centers and judiciously selected ligands are key factors to obtain luminescent Cd MOFs with proper porosity and functional groups to provide potential open Lewis acid or base sites for specific host–guest interactions that can tune the luminescent properties. There are several reported Cd MOFs for sensing functions, which highlight the significance of luminescent MOFs (Table 3). Importantly, a series of $G_n\text{CdL}_2$ ($L = 4\text{-amino-}3,5\text{-bis(4-pyridyl-3-phenyl)-1,2,4-triazole}$; $n = 1, 2$) host–guest complexes reported by Dong et al.^[41] and Cd^{II} –guanazole (3,5-diamino-1,2,4-triazole) hybrid family reported by Yao et al.^[42] exhibit interesting sensing of organic small-molecule solvents and anions, respectively. The porosity and potential open metal/organic group sites within Cd MOFs have played a significant role on their sensing functionality, such as open Cd^{2+} sites for small-molecule sensing, hydrogen-bonding interactions for X^- , and open Lewis basic triazole sites for Cd^{2+} .

The fluorescence sensing ability of **1**, **2**, and **2c** were examined with the addition of different organic compounds to the suspension of the complexes. As shown in Figure 16, the addition of 4000 ppm nitroaromatics, such as NB, *p*-DNB, *m*-DNB, and FNB, could almost quench the emissions of **1**, **2**, and **2c**;

the highest quenching efficiencies were 99.78%, 99.85%, and 99.92%, respectively. With the addition of the same amount of other organic compounds, including alcohols (methanol, ethanol, *n*-propanol, and 2-propanol), amides (DMAC), ketones (acetone), chloroalkanes (CH_2Cl_2 and CHCl_3), nitriles (CH_3CN), nitroaliphatics (e.g., nitromethane (NM) and tris(hydroxymethyl)-nitromethane (THMNM)), and even other aromatic complexes and heterocycles (toluene, pyridine, and morpholine), the maximum change in the emission intensity was no more than 44.3% for **1**, 52.2% for **2**, and 56.5% for **2c**. The properties make complexes **1**, **2**, and **2c** potential fluorescence sensors for nitroaromatic explosives.

To further investigate the sensing properties of **1**, **2** and **2c**, the emissive response was monitored by gradually increasing the *p*-DNB content in emulsions of **1**, **2**, and **2c** dispersed in DMF. As displayed in Figure 17, the emission intensity decreased upon the addition of 5 ppm *p*-DNB and was nearly completely quenched at a concentration of 150 ppm with a high quenching efficiency of 90.6% for **1**, 88.6% for **2**, and 93.4% for **2c**; these values are comparable to other MOF sensors for NB.^[46] For $[\text{Zn}_2(\text{tib})(\text{HL}^1)(\text{H}_2\text{L}^1)_{0.5}] \cdot 2\text{H}_2\text{O}$ (tib = 1,3,5-tris-(1-imidazolyl)benzene; $\text{H}_4\text{L}^1 = \text{biphenyl-}3,3',4,4'\text{-tetracarboxylic}$

Table 3. Selected luminescent Cd MOF materials for sensing applications.

Cd MOF luminescent materials	Luminescent substrates	Ref.
CdL_2 ^[a]	organic small molecules	[41]
$[\text{Cd}(\text{NDC})_{0.5}(\text{PCA})] \cdot \text{Gx}$ ^[b]	TNP	[45]
$[\text{NH}_2(\text{CH}_3)_2]_2[\text{Cd}_{17}(\text{L})_{12}(\mu_3\text{-H}_2\text{O})_4(\text{DMF})_2(\text{H}_2\text{O})_2] \cdot \text{solvent}$ ^[c]	derivatives of NB	[43c]
$[\text{Cd}_5(\text{datrz})_4\text{X}_4(\text{OH})_2]$ ^[d]	anions	[43b]

[a] $L = 4\text{-amino-}3,5\text{-bis(4-pyridyl-3-phenyl)-1,2,4-triazole}$. [b] NDC = 2,6-naphthalenedicarboxylic acid, PCA = 4-pyridinecarboxylic acid, G = guest molecules, TNP = 2,4,6-trinitrophenol. [c] $\text{H}_3\text{L} = 2,4,6\text{-tris[1-(3-carboxyphenoxy)ylmethyl]mesitylene}$. [d] Hdatrz = 3,5-diamino-1,2,4-triazole; X = Cl, Br.

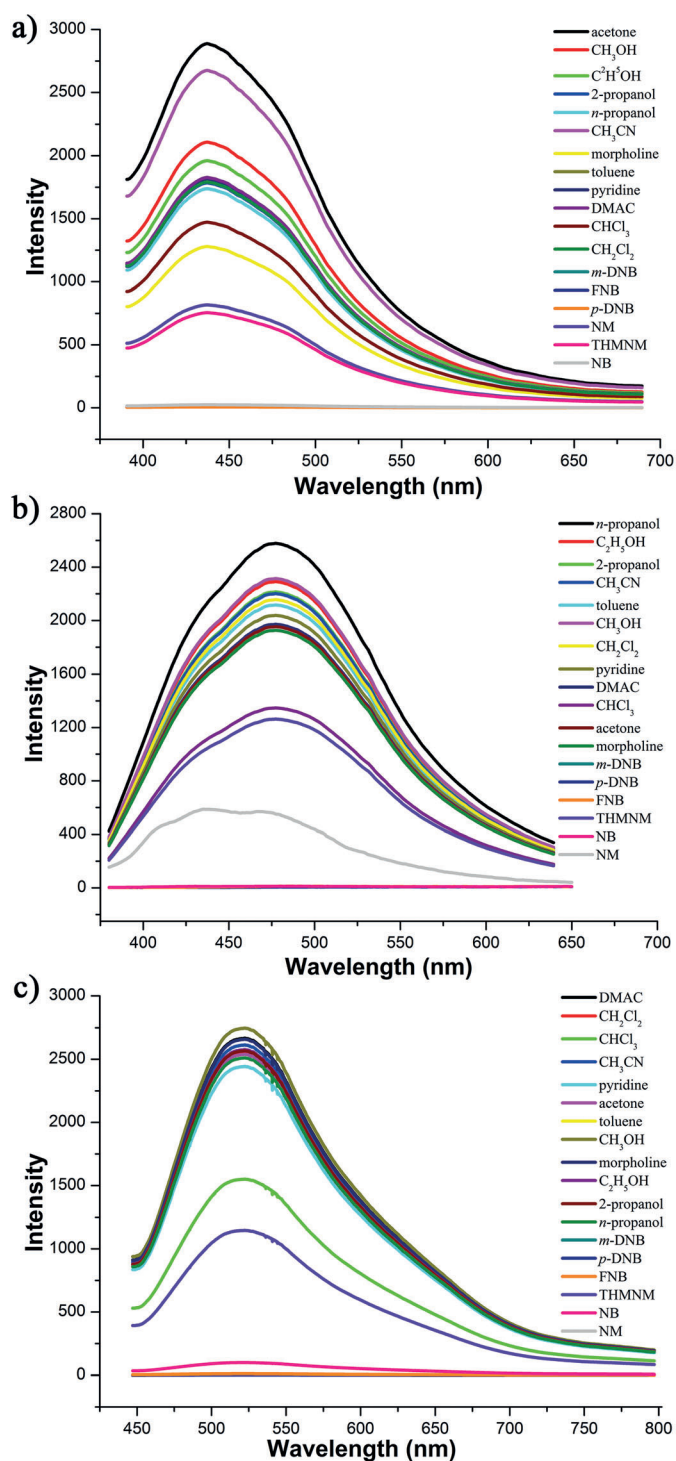


Figure 16. Emission spectra of: a) **1**, b) **2**, and c) **2c** dispersed in DMF with the addition of 4000 ppm of different organic compounds.

acid),^[43a] the photoluminescent intensity decreased to 50% at a concentration of only 200 ppm, which allowed us to detect small amounts of NB in solution. Another 2D Zn^{II} complex, [Zn₂(L)(bipy)(H₂O)₂](H₂O)₃(DMF)₂ (H₄L = bis-(3,5-dicarboxyphenyl)terephthalamide; bipy = 4,4'-bipyridine), reported by Bu's group could selectively detect NB through a redox fluorescence quenching mechanism.^[43b] When the additional amount

of NB was only 2000 ppm, the fluorescence intensity of the suspension of this Zn^{II} complex at $\lambda = 450$ nm was decreased by 90%. Furthermore, another 3D luminescent MOF, [NH₂(CH₃)₂]₂[Cd₁₇(L)₁₂(μ_3 -H₂O)₄(DMF)₂(H₂O)₂]-solvent, shows high sensitivity and a quick response toward the presence of a trace amount of NB in solution or vapor state, which may be used for NB sensing applications.^[43c] Meanwhile, such a 3D Cd^{II} complex can also detect trace amounts of derivatives of nitrobenzene, such as 4-nitrotoluene (4-NT), *m*-DNB, and *p*-DNB. The emission intensity decreased upon the addition of 5 ppm NB and was nearly completely quenched at a concentration of 100 ppm with a high quenching efficiency of 92.5%, which was higher than or comparable to other MOF sensors for NB.^[43a,b,d]

As illustrated in Figures S18–S20, among the six nitro compounds, complexes **1**, **2**, and **2c** are more sensitive to *p*-DNB than five other nitro compounds at room temperature, especially nitroaliphatics, such as NM and THMNM. Complexes **1**, **2**, and **2c** exhibit extremely high detection sensitivity towards *p*-DNB explosives with high quenching efficiencies of 99.78, 99.81, and 99.90%, respectively. To date, several MOF-based fluorescence sensors have been developed for the detection of nitroaromatic explosives. For example, Li et al. reported two highly luminescent MOFs,^[44] [Zn₂(oba)₂(bpy)]·3DMA (H₂oba = 4,4'-oxybis(benzoic acid)) and [Zn₂(bpdc)₂(bpee)]·2DMF (bpdc = 4,4'-biphenyldicarboxylate, bpee = 1,2-bipyridylethene), which exhibit unique selectivity in the detection of nitroaromatics with different groups and high explosives. The excellent fluorescence quenching response to 2,3-dimethyl-2,3-dinitrobutane (DMNB, a taggant required by law in all commercial plastic explosives) can be further attributed to pore confinement of the analyte inside the molecular-sized cavities of such Zn^{II} complexes; this facilitates stronger interactions between DMNB and the host framework, as reflected by the relatively small difference in the quenching percentages for NB, which exhibits only 10% higher sensitivity (94% quenching at 10 s) than that of DMNB. In [Zn₂(oba)₂(bpy)]·3DMA, NB quenches the emission by as much as 84%, and the order of quenching efficiency for selected nitroaromatics is NB > *m*-DNB > NT ≈ *p*-DNB > dinitrotoluene (DNT). Notably, this order is not fully in accordance with the trend of electron-withdrawing groups, but it is fully consistent when the vapor pressure of each analyte is also taken into consideration. The fact that NB exhibits the strongest quenching effect can be attributed to two factors: the high vapor pressure and the strongly electron-withdrawing –NO₂ group. Although the vapor pressure of NT is comparable to that of NB, the quenching efficiency (29%) is significantly less because of the presence of the electron-donating –CH₃ group. Similarly, although *m*- and *p*-DNB have two strongly electron-withdrawing –NO₂ groups, both have very low vapor pressures at room temperature. Interestingly, Ghosh's group demonstrated another luminescent 3D MOF [Cd(NDC)_{0.5}(PCA)]·G_x (G = guest molecules; PCA = 4-pyridinecarboxylic acid) for the highly selective detection of TNP.^[45] To explore the ability of such a Cd^{II} complex to sense a trace quantity of nitro explosives, fluorescence-quenching titrations were performed with the incremental addition of analytes to such

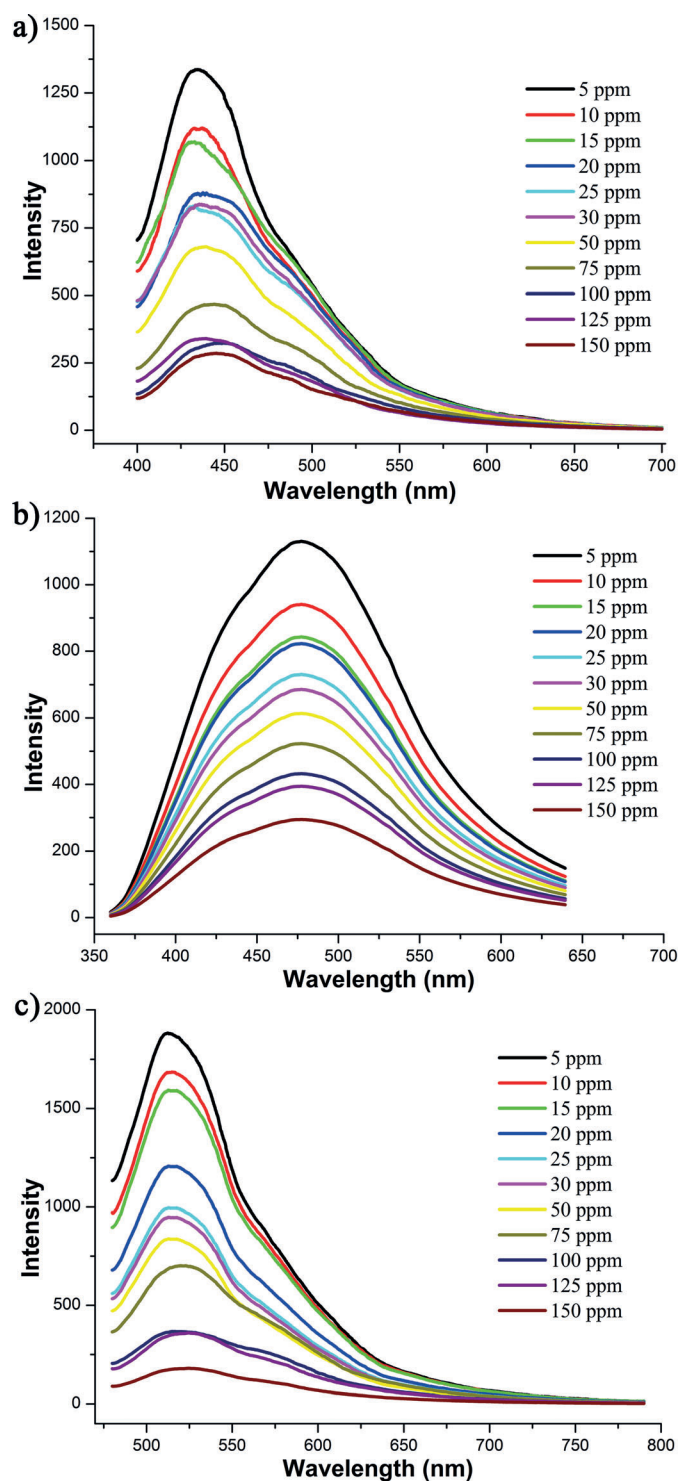


Figure 17. Fluorescence titrations of: a) **1**, b) **2**, and c) **2c** dispersed in DMF with the addition of different concentrations of *p*-DNB.

a Cd^{II} complex dispersed in MeCN. Fast and high fluorescence quenching was observed upon the incremental addition of a solution of TNP (1 mM). The visible bright-blue emission of such a Cd^{II} complex in UV light vanished upon the addition of the solution of TNP, which quenched nearly 78% of the initial fluorescence intensity. Fluorescence quenching by TNP could be easily discerned at a low concentration (4 μM). Fluorescence

quenching titrations were also performed with nitroaromatics, such as 2,4,6-trinitrotoluene (TNT), 2,4-DNT, 2,6-DNT, *m*-DNB, and NB, and nitroaliphatic compounds, such as DMNB, NM, and 1,3,5-trinitro-1,3,5-triazacyclohexane. All other nitro compounds showed little effect on the fluorescence intensity. These results demonstrate that such a Cd^{II} complex has high selectivity for TNP compared with other nitro compounds.

As shown in Figure 16, among the tested aromatic organic compounds (toluene, benzene, and nitro compounds), the emissions of **1**, **2**, and **2c** can only be quenched by nitroaromatic explosives. Therefore, the fluorescence responses of **1**, **2**, and **2c** to nitro compound explosives were attributed to the electron-transfer quenching mechanism, that is, in the presence of nitro compounds, the excited electron of complexes **1**, **2**, and **2c** would undergo a transfer to nitro compounds, instead of relaxation to the ground state with fluorescence emission. Because the photoluminescence of **1**, **2**, and **2c** originated from the ligand, the sensitive response of **1**, **2**, and **2c** to nitroaromatic explosives could be attributed to the electron-rich properties of the ligand, which facilitated the excited-state electron-transfer process. Although there are cavities in the framework of **1**, the absence of an accessible path excludes the possibility of analyte encapsulation during the sensing process. Therefore, the sensing mechanism of **1** should be not guest-induced quenching, in which analyte molecules are included in the pores as guests and interact directly with the fluorophore.

Cyanide poisoning is less frequent than mercury or strychnine poisoning, although during recent years the death rate from cyanide poisoning has been increasing. Cyano-containing molecules show interesting reactivity due to the strong electron-withdrawing capability of the cyano group.^[46] Cyano complexes are also hypothesized to be intermediates in the formation of biologically relevant molecules.^[47,48] However, none of the complexes proved active against the replication of retroviruses (human immunodeficiency virus, murine sarcoma virus) at concentrations that were not toxic to the host cells. Ferric heme systems can be ligated by CN⁻, a strong-field ligand, which places the heme into a low-spin state that is generally thought to be very stable and that does not undergo photodissociation.^[49] Therefore, the development of the detection of the cyano group is very important for environmental and safety considerations. Additionally, the application of MOFs for the sensing of cyano groups is limited because most porous MOFs used for the detection of cyano groups must be activated to evacuate the pores before sensing because the presence of solvent or other guest molecules diminishes the performance of the MOFs. On the other hand, the introduction of electron-rich aromatic ligands could improve sensor performances effectively because quenching sensing is generally realized by the transfer of photoexcited electrons from the MOFs to the electron-deficient analytes. Inspired by our previous experiences,^[50] we now carry out our work in the field of selective recognition toward cyano-containing molecules.

The fluorescent sensing ability of **2** was first examined with the addition of different molecules to a suspension of **2**. The addition of cyano-containing molecules, such as K₄[W(CN)₆],

$K_3[Mn(CN)_6]$, $Na_3[W(CN)_6]$, $Na_3[Mo(CN)_6]$, $Cs_3[W(CN)_6]$, $[NBu_3][Mo(CN)_6]$, $[NBu_3][W(CN)_6]$, and $Rb_3[W(CN)_6]$, at 400 ppm could almost entirely quench the emission of **2** (Figure 18). The maximum decrease in the emission intensity was more than 99.85% with the addition of $[NBu_3][Mo(CN)_6]$, which indicated that **2** had a selective response to cyano-containing molecules, especially to $[NBu_3][Mo(CN)_6]$. To investigate the sensing properties of **2** further, the emissive response was monitored by gradually increasing the $[NBu_3][Mo(CN)_6]$ content of emulsions of **2** dispersed in DMF. The emission intensity decreased upon the addition of 5 ppm of $[NBu_3][Mo(CN)_6]$ and was nearly completely quenched at a concentration of 100 ppm, with a high quenching efficiency of 99.95% (Figure S22). To the best of our knowledge, no other examples of selective sensors toward cyano-containing molecules have been reported.^[51] The emissions of **2** can be quenched by cyano-containing molecules. Therefore, the fluorescence responses of **1** to cyano-containing molecules were attributed to the electron-transfer quenching mechanism, that is, in the presence of cyano-containing molecules, the excited electron of **1** would undergo transfer to the cyano complex, instead of relaxation to the ground state with fluorescence emission. Because the photoluminescence of **1** originates from the ligand, the sensitive response of **1** to cyano complexes can be attributed to the electron-rich properties of the ligand, which facilitate the excited-state electron-transfer process. Although there are cavities in the framework of **1**, the absence of an accessible path excludes the possibility of analyte encapsulation during the sensing process. Therefore, the sensing mechanism of **1** should not be guest-induced quenching, in which analyte molecules are included in the pores as guests and interact directly with the fluorophore.

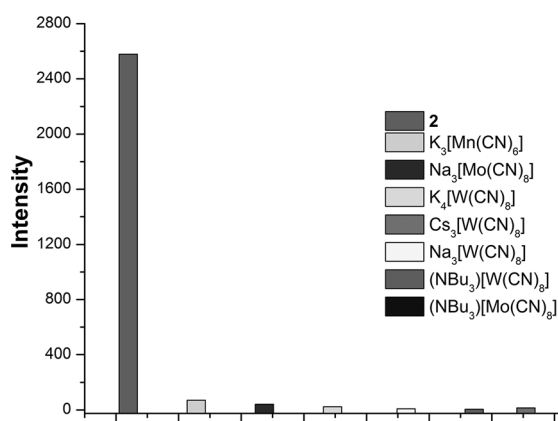


Figure 18. Emission intensities of **2** in DMF with different cyano complexes.

Conclusions

A new bidentate ligand, TPPT, has been designed and synthesized. By using TPPT as a building block in self-assembly with $Cd(NO_3)_2 \cdot 4H_2O$ and $CdCl_2 \cdot 10.5H_2O$, novel 1D double-chain **1** and 2D (4,4)-layer **2** have been constructed. Anion-exchange experiments for **2** occurred in a SC–SC transformation manner. Luminescent measurements indicate that **1** is the first example

of a triazole derivative as a luminescent probe of Ca^{2+} . Moreover, the luminescent emissions of **1**, **2**, and **2c** could be quenched by trace amounts of nitroaromatic explosives, such as *m*-DNB, NB, and FNB. The quenching mechanism is attributed to electron transfer from the excited-state electron-donating MOF framework to electron-withdrawing nitroaromatic explosives, as well as the dispersible nature of the MOF particles.

Experimental Section

Materials and methods

All reagents are commercially available and used without further purification. The elemental analysis of C, N, and H has been measured on a PerkinElmer 240 elemental analyzer. The photoluminescence spectra have been recorded by using an MPF-4 fluorescence spectrophotometer with a xenon arc lamp as the light source. Powder XRD analysis has been determined on a D/Max-2500 X-ray diffractometer by using $Cu_{K\alpha}$ radiation. The photoluminescence spectra were recorded by using an MPF-4 fluorescence spectrophotometer with a xenon arc lamp as the light source. 1H NMR spectra have been measured by using a Bruker Avance 400 MHz spectrometer. Chemical shifts are reported in δ relative to tetramethylsilane (TMS). Thermal analyses (under an oxygenated atmosphere at a heating rate of $5^\circ C min^{-1}$) were carried out by using a Labsys NETZSCH TG 209 Setaram apparatus. The fluorescence quantum yields of complexes **1**, **1a**, **1b**, **2**, **2a**, **2b**, and **2c** were measured by using an Edinburgh Instruments FLS 920 device.

Caution! Nitroaromatics, such as NB, *m*-DNB, and *p*-DNB, and nitroaliphatics, such as NM and THMNM, are highly explosive and should be handled carefully and in small amounts.

X-ray crystallography

Single-crystal XRD determination was performed on an APEX II CCD area detector and a Bruker Smart CCD diffractometer. A graphite crystal monochromator was equipped in the incident beam for data collection at a temperature of 296(2) K for TPPT, **1**, **2**, **2a**, **2b**, and **2c** and at 173(2) K for **1a**, **1b**, and **2**. The ω - φ scan technique was applied. Direct methods were applied to solve the structures. Full-matrix least-squares methods by using the SHELXL-97 and SHELXS-97 programs were used to refine the crystal structures.^[52,53] For all coordination complexes, anisotropic thermal parameters were applied to all non-hydrogen atoms. Anomalous dispersion corrections were incorporated and analytical expressions of neutral-atom scattering factors were also used. These crystallographic data, selected bond lengths, and bond angles of these complexes are listed in Tables 1 and 2.

CCDC-1424630 (TPPT), 1016243 (**1**), 1055207 (**1a**), 1016244 (**1b**), 1044214 (**2**), 1016246 (**2a**), 1016247 (**2b**), and 1016248 (**2c**) contain the supplementary crystallographic data for this paper. These data are provided free of charge by The Cambridge Crystallographic Data Centre.

Synthesis of 4,4'-dibromodiphenyl ether

4,4'-Dibromodiphenyl ether was prepared by reacting an excess of Br_2 with diphenyl ether in methanol. Br_2 (3.99 g) was added dropwise to diphenyl ether (2.04 g), which was dissolved in methanol (10 mL). The reaction mixture was then stirred at $60^\circ C$ for an additional 1 h. After cooling to room temperature, the product precipitated. Yield: 70%; m.p. 59 – $61^\circ C$.

Synthesis of TPPT

The synthetic method used to prepare TPPT was the same as that reported previously.^[54] A mixture of 4,4'-dibromodiphenyl ether (1.63 g, 5 mmol), 1*H*-1,2,4-triazole (0.69 g, 10 mmol), potassium carbonate (5.52 g, 40 mmol), and CuO (0.16 g, 2 mmol) were heated with stirring in DMSO (20 mL) at 150 °C for 48 h. The resulting slurry was cooled to room temperature and solids were removed by filtration. DMSO was removed by distillation under reduced pressure. Dichloromethane was added to the remaining filtrate and the mixture was then washed with water and dried over sodium sulfate. Dichloromethane was then removed. The products were recrystallized in methanol and water, and light-yellow solids were obtained. Yield: 12%; m.p. 192–195 °C. As shown in Figure S21 in the Supporting Information, ¹H NMR (400 MHz, CDCl₃): δ = 8.56 (s, 2H), 8.12 (s, 2H), 7.68–7.70 (d, 4H), 7.17–7.20 ppm (d, 4H). TPPT (0.0304 g, 0.1 mmol) was dissolved in CH₂Cl₂ and CH₃OH (1:1 v/v). Under slow evaporation of the filtrate at room temperature, well-shaped colorless crystals of TPPT suitable for XRD were obtained within one month in 90% yield. Elemental analysis calcd (%) for C₁₆N₆OH₁₂: C 63.15, H 3.97, N 27.62; found: C 63.19, H 4.06, N 27.50.

Synthesis of 1

Complex **1** was prepared by slow diffusion at room temperature of a solution of TPPT (0.0609 g, 0.2 mmol) in CHCl₃ (10 mL) at the bottom of the tube and CH₃OH (4 mL) containing Cd(NO₃)₂·6H₂O (0.1164 g, 0.4 mmol) on the top. After a few weeks, well-shaped yellow rodlike crystals suitable for X-ray analysis were obtained. Yield: 30%; elemental analysis calcd (%) for C₃₂H₃₀CdN₁₄O₁₁: C 42.75, H 3.36, N 21.81; found: C 42.72, H 3.38, N 21.79.

Synthesis of 1 a

A suspension of **1** (0.2628 g, 0.5 mmol) in DMF (10 mL) was stirred for 6 h. Through our careful observations, well-shaped yellow rodlike crystals dissolved and brown block crystals suitable for XRD analysis were isolated after one week. Yield: 45%; elemental analysis calcd (%) for C₃₅H₃₁CdN₁₅O₉: C 45.79, H 3.40, N 22.88; found: C 45.88, H 3.37, N 22.80.

Synthesis of 1 b

A suspension of **1** or **1 a** (0.5 mmol) in DMAC (10 mL) was stirred for 6 h. Through our careful observations, well-shaped yellow rodlike crystals dissolved and brown block crystals suitable for XRD analysis were isolated after two weeks. Well-shaped brown block crystals suitable for XRD analysis were isolated. Yield: 35%; elemental analysis calcd (%) for C₃₆H₃₃CdN₁₅O₉: C 46.39, H 3.57, N 22.54; found: C 46.45, H 3.64, N 22.51.

Synthesis of 2

A mixture of CdCl₂·10.5H₂O (0.0745 g, 0.2 mmol), TPPT (0.0304 g, 0.1 mmol), CHCl₃ (1 mL), H₂O (1 mL), and CH₃OH (8 mL) was placed in a stainless-steel vessel (23.0 mL) and then heated to 120 °C for 3 days, and cooled to room temperature at a rate of 10 °C h⁻¹. Colorless block crystals suitable for X-ray analysis were directly obtained. Yield: 25%; elemental analysis calcd (%) for C₁₆H₁₄CdCl₂N₆O₂: C 38.01, H 2.79, N 16.62; found: C 37.94, H 2.66, N 16.56.

Synthesis of 2 a

A suspension mixture of **2** (0.5 mmol) and NaBr (5 mmol) in CHCl₃/C₂H₅OH/H₂O (1:8:2 v/v/v; 11 mL) was stirred for 6 h. Well-shaped colorless block crystals suitable for XRD analysis were isolated. Yield: 30%; elemental analysis calcd (%) for C₁₈H₁₈Br₂CdN₆O₂: C 34.72, H 2.91, N 13.50; found: C 34.68, H 2.87, N 13.56.

Synthesis of 2 b

A suspension of **2** (0.5 mmol) and NaI (5 mmol) in CHCl₃/C₂H₅OH/H₂O (v/v/v 1:8:2; 11 mL) was stirred for 6 h. Well-shaped colorless block crystals suitable for XRD analysis were isolated. Yield: 32%; elemental analysis calcd (%) for C₃₃H₂₅CdCl₃I₂N₁₂O₂: C 40.37, H 2.57, N 17.12; found: C 40.28, H 2.22, N 17.33.

Synthesis of 2 c

A suspension of **2** (0.5 mmol) and NaOAc (5 mmol) in CHCl₃/C₂H₅OH/H₂O (v/v/v 1:8:2; 11 mL) was stirred for 6 h. Well-shaped colorless block crystals suitable for XRD analysis were isolated. Yield: 40%; elemental analysis calcd (%) for C₂₀H₂₂CdN₆O₇: C 42.08, H 3.88, N 14.72; found: C 42.10; H 3.97, N 14.76.

Acknowledgements

This work was supported financially by the NSFC (41372373, 21421001, 21471113 and 21531005), the innovation team plan of the Tianjin Education Committee (TD12-5037), and the Opening Fund of Key Laboratory of Advanced Energy Materials Chemistry (Ministry of Education), Nankai University.

Keywords: crystal growth · fluorescence · metal–organic frameworks · self-assembly · sensors

- [1] H.-C. Zhou, J. R. Long, O. M. Yaghi, *Chem. Rev.* **2012**, *112*, 673–1268.
- [2] P. Guo, D. Dutta, A. G. Wong-Foy, D. W. Gidley, A. J. Matzger, *J. Am. Chem. Soc.* **2015**, *137*, 2651–2657.
- [3] S. S. Park, E. R. Hontz, L. Sun, C. H. Hendon, A. Walsh, T. V. Voorhis, M. Dincă, *J. Am. Chem. Soc.* **2015**, *137*, 1774–1777.
- [4] L. E. Kreno, K. Leong, O. K. Farha, M. Allendorf, R. P. Van Duyne, J. T. Hupp, *Chem. Rev.* **2012**, *112*, 1105–1125.
- [5] X. Kuang, X. Wu, R. Yu, J. P. Donahue, J. Huang, C.-Z. Lu, *Nat. Chem.* **2010**, *2*, 461–465.
- [6] X. Zhao, X. Bu, Q.-G. Zhai, H. Tran, P. Feng, *J. Am. Chem. Soc.* **2015**, *137*, 1396–1399.
- [7] Y.-B. Zhang, H. Furukawa, N. Ko, W. Nie, H. J. Park, S. Okajima, K. E. Cordova, H. Deng, J. Kim, O. M. Yaghi, *J. Am. Chem. Soc.* **2015**, *137*, 2641–2650.
- [8] A. J. Fletcher, K. M. Thomas, M. J. Rosseinsky, *J. Solid State Chem.* **2005**, *178*, 2491–2510.
- [9] G. Lu, J. T. Hupp, *J. Am. Chem. Soc.* **2010**, *132*, 7832–7833.
- [10] S. Horike, S. Shimomura, S. Kitagawa, *Nat. Chem.* **2009**, *1*, 695–704.
- [11] a) M. Kawano, M. Fujita, *Coord. Chem. Rev.* **2007**, *251*, 2592–2605; b) S. Kitagawa, R. Matsuda, *Coord. Chem. Rev.* **2007**, *251*, 2490–2509; c) T. K. Maji, R. S. Kitagawa, *Nat. Mater.* **2007**, *6*, 142–148; d) H. J. Park, D.-W. Lim, W. S. Yang, T.-R. Oh, M. P. Suh, *Chem. Eur. J.* **2011**, *17*, 7251–7260.
- [12] a) S. Kitagawa, K. Uemura, *Chem. Soc. Rev.* **2005**, *34*, 109–119; b) Q. Chen, Z. Chang, W.-C. Song, H. Song, H.-B. Song, T.-L. Hu, X.-H. Bu, *Angew. Chem. Int. Ed.* **2013**, *52*, 11550–11553; *Angew. Chem.* **2013**, *125*, 11764–11767; c) C. H. Hu, U. Englert, *Angew. Chem. Int. Ed.* **2005**, *44*, 2281–2283; *Angew. Chem.* **2005**, *117*, 2321–2323; d) Y. J. Zhang, T. Liu, S. Kanegawa, O. Sato, *J. Am. Chem. Soc.* **2009**, *131*, 7942–7943.
- [13] a) C. D. Wu, W. B. Lin, *Angew. Chem. Int. Ed.* **2005**, *44*, 1958–1961; *Angew. Chem.* **2005**, *117*, 1994–1997; b) E. Y. Lee, M. P. Suh, *Angew.*

- Chem. Int. Ed.* **2004**, *43*, 2798–2801; *Angew. Chem.* **2004**, *116*, 2858–2861; c) J. Sun, F. Dai, W. Yuan, W. Bi, X. Zhao, W. Sun, D. Sun, *Angew. Chem. Int. Ed.* **2011**, *50*, 7061–7064; *Angew. Chem.* **2011**, *123*, 7199–7202; d) M. Eddaoudi, J. Kim, N. Rosi, D. Vodak, J. Wachter, M. O’Keeffe, O. M. Yaghi, *Science* **2002**, *295*, 469–472.
- [14] a) Y. Wang, P. Cheng, Y. Song, D.-Z. Liao, S.-P. Yan, *Chem. Eur. J.* **2007**, *13*, 8133–8138; b) Y. Wang, B. Yuan, Y.-Y. Xu, X.-G. Wang, B. Ding, X.-J. Zhao, *Chem. Eur. J.* **2015**, *21*, 2107–2116; c) J.-Y. Liu, Q. Wang, L.-J. Zhang, B. Yuan, Y.-Y. Xu, X. Zhang, C.-Y. Zhao, D. Wang, Y. Yuan, Y. Wang, B. Ding, X.-J. Zhao, M.-M. Yue, *Inorg. Chem.* **2014**, *53*, 5972–5985.
- [15] a) M. M. Wanderley, C. Wang, C.-D. Wu, W. Lin, *J. Am. Chem. Soc.* **2012**, *134*, 9050–9053; b) N. B. Shustova, A. F. Cozzolino, S. Reineke, M. Baldo, M. Dincă, *J. Am. Chem. Soc.* **2013**, *135*, 13326–13329; c) Z.-Z. Lu, R. Zhang, Y.-Z. Li, Z.-J. Guo, H.-G. Zheng, *J. Am. Chem. Soc.* **2011**, *133*, 4172–4174; d) Y. Guo, X. Feng, T. Han, S. Wang, Z. Lin, Y. Dong, B. Wang, *J. Am. Chem. Soc.* **2014**, *136*, 15485–15488.
- [16] a) K. Jayaramulu, R. P. Narayanan, S. J. George, T. K. Maji, *Inorg. Chem.* **2012**, *51*, 10089–10091; b) C.-X. Yang, H.-B. Ren, X.-P. Yan, *Anal. Chem.* **2013**, *85*, 7441–7446; c) J.-S. Qin, S.-R. Zhang, D.-Y. Du, P. Shen, S.-J. Bao, Y.-Q. Lan, Z.-M. Su, *Chem. Eur. J.* **2014**, *20*, 5625–5630; d) Z.-B. Han, Z.-Z. Xiao, M. Hao, D.-Q. Yuan, L. Liu, N. Wei, H.-M. Yao, M. Zhou, *Cryst. Growth Des.* **2015**, *15*, 531–533; e) J. Cao, Y. Gao, Y. Wang, C. Du, Z. Liu, *Chem. Commun.* **2013**, *49*, 6897–6899; f) S. Bhattacharyya, A. Chakraborty, K. Jayaramulu, A. Hazra, T. K. Maji, *Chem. Commun.* **2014**, *50*, 13567–13570; g) Z. Xiang, C. Fang, S. Leng, D. Cao, *J. Mater. Chem. A* **2014**, *2*, 7662–7665; h) J.-N. Hao, B. Yan, *J. Mater. Chem. C* **2014**, *2*, 6758–6764; i) M. Zheng, H. Tan, Z. Xie, L. Zhang, X. Jing, Z. Sun, *ACS Appl. Mater. Interfaces* **2013**, *5*, 1078–1083; j) X.-Y. Xu, B. Yan, *ACS Appl. Mater. Interfaces* **2015**, *7*, 721–729; k) Q. Tang, S. Liu, Y. Liu, J. Miao, S. Li, L. Zhang, Z. Shi, Z. Zheng, *Inorg. Chem.* **2013**, *52*, 2799–2801; l) Z. Chen, Y. Sun, L. Zhang, D. Sun, F. Liu, Q. Meng, R. Wang, D. Sun, *Chem. Commun.* **2013**, *49*, 11557–11559; m) B. Chen, L. Wang, Y. Xiao, F. R. Fronczek, M. Xue, Y. Cui, G. Qian, *Angew. Chem. Int. Ed.* **2009**, *48*, 500–503; *Angew. Chem.* **2009**, *121*, 508–511.
- [17] a) S. Pramanik, C. Zheng, X. Zhang, T. J. Emge, J. Li, *J. Am. Chem. Soc.* **2011**, *133*, 4153–4155; b) Z. Hu, B. J. Deibert, J. Li, *Chem. Soc. Rev.* **2014**, *43*, 5815–5840; c) T. K. Kim, J. H. Lee, D. Moon, H. R. Moon, *Inorg. Chem.* **2013**, *52*, 589–595; d) D. K. Singha, S. Bhattacharya, P. Majee, S. K. Mondal, M. Kumar, P. Mahata, *J. Mater. Chem. A* **2014**, *2*, 20908–20915.
- [18] J. Rocha, L. D. Carlos, F. A. A. Paz, D. Ananias, *Chem. Soc. Rev.* **2011**, *40*, 926–940.
- [19] P. Alborés, E. Rentschler, *Angew. Chem. Int. Ed.* **2009**, *48*, 9366–9370; *Angew. Chem.* **2009**, *121*, 9530–9534.
- [20] a) M. H. Klingele, S. Brooker, *Coord. Chem. Rev.* **2003**, *241*, 119–132; b) S. Ferrer, J. G. Haasnoot, J. Reedijk, E. Müller, M. B. M. A. Cingi, M. Lanfranchi, M. Lanfredi, J. Ribas, *Inorg. Chem.* **2000**, *39*, 1859–1867; c) J. P. Zhang, X. M. Chen, *Chem. Commun.* **2006**, *16*, 1689–1699.
- [21] B. Ding, L. Yi, Y. Wang, P. Cheng, D.-Z. Liao, S.-P. Yan, Z.-H. Jiang, H.-B. Song, H.-G. Wang, *Dalton Trans.* **2006**, *36*, 665–675.
- [22] S. Hou, Q.-K. Liu, J.-P. Ma, Y.-B. Dong, *Inorg. Chem.* **2013**, *52*, 3225–3235.
- [23] a) T. Hoang, J. W. Lauher, F. W. Fowler, *J. Am. Chem. Soc.* **2002**, *124*, 10656–10657; b) K. Hanson, N. Calin, D. Bugaris, M. Scancella, S. C. Sevov, *J. Am. Chem. Soc.* **2004**, *126*, 10502–10503.
- [24] a) J. J. Vittal, *Coord. Chem. Rev.* **2007**, *251*, 1781–1795; b) M. Nihei, L. Q. Han, H. Oshio, *J. Am. Chem. Soc.* **2007**, *129*, 5312–5313; c) M. P. Suh, J. W. Ko, H. J. Choi, *J. Am. Chem. Soc.* **2002**, *124*, 10976–10977; d) D. Liu, Z. G. Ren, H. X. Li, J. P. Lang, N. Y. Li, B. F. Abrahams, *Angew. Chem. Int. Ed.* **2010**, *49*, 4767–4770; *Angew. Chem.* **2010**, *122*, 4877–4880; e) O. V. Zenkina, E. C. Keske, R. Wang, C. M. Crudden, *Angew. Chem. Int. Ed.* **2011**, *50*, 8100–8104; *Angew. Chem.* **2011**, *123*, 8250–8254; f) Y. C. Ou, W. T. Liu, J. Y. Li, G. G. Zhang, J. Wang, M. L. Tong, *Chem. Commun.* **2011**, *47*, 9384–9386.
- [25] P. B. Chatterjee, A. Audhya, S. Bhattacharya, S. M. T. Abtbat, K. Bhattacharya, M. Chaudhury, *J. Am. Chem. Soc.* **2010**, *132*, 15842–15845.
- [26] a) M. C. Bernini, F. Gándara, M. Iglesias, N. Snejkó, E. Gutiérrez-Puebla, E. V. Brusau, G. E. Narda, M. Á. Monge, *Chem. Eur. J.* **2009**, *15*, 4896–4905; b) J. Y. Lee, S. Y. Lee, W. Sim, K. M. Park, J. Kim, S. S. Lee, *J. Am. Chem. Soc.* **2008**, *130*, 6902–6903; c) J. P. Zhang, Y. Y. Lin, W. X. Zhang, X. M. Chen, *J. Am. Chem. Soc.* **2005**, *127*, 14162–14163.
- [27] a) J. Fu, H. Li, Y. Mu, H. Hou, Y. Fan, *Chem. Commun.* **2011**, *47*, 5271–5273; b) K. Raatikainen, K. Rissanen, *Chem. Sci.* **2012**, *3*, 1235–1239; c) Y. Han, H. Xu, Y. Liu, H. Li, H. Hou, Y. Fan, S. R. Batten, *Chem. Eur. J.* **2012**, *18*, 13954–13958; d) J. J. Jiang, L. Li, M. H. Lan, M. Pan, A. Eichhofer, D. Fenske, C. Y. Su, *Chem. Eur. J.* **2010**, *16*, 1841–1848; e) C. Massera, M. Melegari, E. Kalenius, F. Ugozzoli, E. Dalcanale, *Chem. Eur. J.* **2011**, *17*, 3064–3068; f) I. H. Park, S. S. Lee, J. J. Vittal, *Chem. Eur. J.* **2013**, *19*, 2695–2702; g) S. Hu, K. H. He, M. H. Zeng, H. H. Zou, Y. M. Jiang, *Inorg. Chem.* **2008**, *47*, 5218–5224; h) H. J. Choi, M. P. Suh, *J. Am. Chem. Soc.* **2004**, *126*, 15844–15851; i) L. Dobrzańska, G. O. Lloyd, H. G. Raubenheimer, L. J. Barbour, *J. Am. Chem. Soc.* **2006**, *128*, 698–699; j) D. Liu, J. P. Lang, B. F. Abrahams, *J. Am. Chem. Soc.* **2011**, *133*, 11042–11045; k) M. H. Zeng, Q. X. Wang, Y. X. Tan, S. Hu, H. X. Zhao, L. S. Long, M. Kurmoo, *J. Am. Chem. Soc.* **2010**, *132*, 2561–2563; l) Y.-Q. Chen, G. R. Li, Z. Chang, Y. K. Qu, Y. H. Zhang, X. H. Bu, *Chem. Sci.* **2013**, *4*, 3678–3682.
- [28] D. Yuan, D. Zhao, D. J. Timmons, H. C. Zhou, *Chem. Sci.* **2011**, *2*, 103–106.
- [29] a) G. Xu, G. C. Guo, M. S. Wang, Z. J. Zhang, W. T. Chen, J. S. Huang, *Angew. Chem. Int. Ed.* **2007**, *46*, 3249–3251; *Angew. Chem.* **2007**, *119*, 3313–3315; b) P. C. Jhang, N. T. Chuang, S. L. Wang, *Angew. Chem. Int. Ed.* **2010**, *49*, 4200–4204; *Angew. Chem.* **2010**, *122*, 4296–4300; c) Q. Chu, D. C. Swenson, L. R. MacGillivray, *Angew. Chem. Int. Ed.* **2005**, *44*, 3569–3572; *Angew. Chem.* **2005**, *117*, 3635–3638; d) C. Avendano, Z. Zhang, A. Ota, H. Zhao, K. R. Dunbar, *Angew. Chem. Int. Ed.* **2011**, *50*, 6543–6547; *Angew. Chem.* **2011**, *123*, 6673–6677.
- [30] X. Xue, X.-S. Wang, R.-G. Xiong, X. Z. You, B. F. Abrahams, C.-M. Che, H.-X. Ju, *Angew. Chem. Int. Ed.* **2002**, *41*, 2944–2946; *Angew. Chem.* **2002**, *114*, 3068–3070.
- [31] a) E. Deiters, V. Bulach, M. W. Hosseini, *Chem. Commun.* **2005**, *31*, 3906–3908; b) L. Dobrzańska, G. O. Lloyd, C. Esterhuysen, L. J. Barbour, *Angew. Chem. Int. Ed.* **2006**, *45*, 5856–5859; *Angew. Chem.* **2006**, *118*, 5988–5991; c) S. Kitagawa, S. Noro, T. Nakamura, *Chem. Commun.* **2006**, *7*, 701–707; d) A. S. R. Chesman, D. R. Turner, G. B. Deacon, S. R. Batten, *Chem. Commun.* **2010**, *46*, 4899–4901.
- [32] a) M. R. Warren, S. K. Brayshaw, A. L. Johnson, S. Schiffrs, P. R. Raithby, T. L. Easun, M. W. George, J. E. Warren, S. J. Teat, *Angew. Chem. Int. Ed.* **2009**, *48*, 5711–5714; *Angew. Chem.* **2009**, *121*, 5821–5824; b) X.-N. Cheng, W.-X. Zhang, X.-M. Chen, *J. Am. Chem. Soc.* **2007**, *129*, 15738–15739; c) S. M. Neville, G. J. Halder, K. W. Chapman, M. B. Duriska, P. D. Southon, J. D. Cashion, J. F. Létard, B. K. Moubaraki, S. Murray, C. J. Kepert, *J. Am. Chem. Soc.* **2008**, *130*, 2869–2876.
- [33] a) S. R. Seidel, P. J. Stang, *Acc. Chem. Res.* **2002**, *35*, 972–983; b) J. L. Boyer, M. L. Kuhlman, T. B. Rauchfuss, *Acc. Chem. Res.* **2007**, *40*, 233–242; c) B. Therrien, G. Süß-Fink, P. Govindaswamy, A. K. Renfrew, P. J. Dyson, *Angew. Chem. Int. Ed.* **2008**, *47*, 3773–3776; *Angew. Chem.* **2008**, *120*, 3833–3836.
- [34] S. R. Halper, L. Do, J. R. Stork, S. M. Cohen, *J. Am. Chem. Soc.* **2006**, *128*, 15255–15268.
- [35] a) Y. Wang, P. Cheng, Y. Song, D. Z. Liao, S. P. Yan, *Chem. Eur. J.* **2007**, *13*, 8131–8138; b) J. Seo, R. Matsuda, H. Sakamoto, C. Bonneau, S. Kitagawa, *J. Am. Chem. Soc.* **2009**, *131*, 12792–12800; c) L. Ma, C. D. Wu, M. M. Wanderley, W. Lin, *Angew. Chem. Int. Ed.* **2010**, *49*, 8244–8248; *Angew. Chem.* **2010**, *122*, 8420–8424; d) M. H. Mir, L. L. Koh, G. K. Tan, J. J. Vittal, *Angew. Chem. Int. Ed.* **2010**, *49*, 390–393; *Angew. Chem.* **2010**, *122*, 400–403.
- [36] a) G. J. Halder, C. J. Kepert, B. Moubaraki, K. S. Murray, J. D. Cashion, *Science* **2002**, *298*, 1762–1765; b) K. Ono, M. Yoshizawa, M. Akita, T. Kato, Y. Tsunobuchi, S.-I. Ohkoshi, M. Fujita, *J. Am. Chem. Soc.* **2009**, *131*, 2782–2783; c) P. D. Southon, L. Liu, E. A. Fellows, D. J. Price, G. J. Halder, K. W. Chapman, B. K. Moubaraki, S. Murray, J.-F. Létard, C. J. Kepert, *J. Am. Chem. Soc.* **2009**, *131*, 10998–11009.
- [37] a) S. J. Dalgarno, S. A. Tucker, D. B. Bassil, J. L. Atwood, *Science* **2005**, *309*, 2037–2039; b) Y.-B. Dong, P. Wang, J.-P. Ma, X.-X. Zhao, H.-Y. Wang, B. Tang, R.-Q. Huang, *J. Am. Chem. Soc.* **2007**, *129*, 4872–4873; c) G. J. McManus, J. J. Perry, M. Perry, B. D. Wagner, M. J. Zaworotko, *J. Am. Chem. Soc.* **2007**, *129*, 9094–9101; d) P. Wang, J.-P. Ma, Y.-B. Dong, R.-Q. Huang, *J. Am. Chem. Soc.* **2007**, *129*, 10620–10621; e) P. Wang, J.-P. Ma, Y.-B. Dong, *Chem. Eur. J.* **2009**, *15*, 10432–10445; f) Y.-Y. Jiang, S.-K. Ren, J.-P. Ma, Q.-K. Liu, Y.-B. Dong, *Chem. Eur. J.* **2009**, *15*, 10742–10746.
- [38] a) D. Maspoch, N. Domingo, N. Roques, K. Wurst, J. Tejada, C. Rovira, D. Ruiz-Molina, J. Veciana, *Chem. Eur. J.* **2007**, *13*, 8153–8163; b) U. H. F. Bunz, *Chem. Rev.* **2000**, *100*, 1605–1644; c) B. C. Tzeng, T. H. Chiu, B. S. Chen, G. H. Lee, *Chem. Eur. J.* **2008**, *14*, 5237–5245.

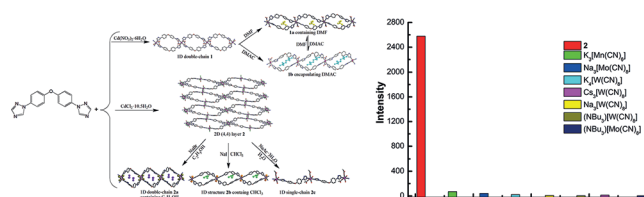
- [39] J. G. Haasnoot, *Coord. Chem. Rev.* **2000**, *200–202*, 131–185.
- [40] a) M. Crit. Harada, *Rev. Toxicol.* **1995**, *25*, 1–24; b) A. J. Cohen, H. Ross Anderson, B. Ostro, K. D. Pandey, M. Krzyzanowski, N. Kunzli, K. Gutschmidt, A. Pope, I. Romieu, J. M. Samet, K. Smith, *J. Toxicol. Environ. Health Part A* **2005**, *68*, 1301–1307; c) M. Kampa, E. Castanas, *Environ. Pollut.* **2008**, *151*, 362–367; d) J. L. Martinez, *Environ. Pollut.* **2009**, *157*, 2893–2902.
- [41] Q.-K. Liu, J.-P. Ma, Y.-B. Dong, *J. Am. Chem. Soc.* **2010**, *132*, 7005–7017.
- [42] R.-B. Zhang, Z.-J. Li, Y.-Y. Qin, J.-K. Cheng, J. Zhang, Y.-G. Yao, *Inorg. Chem.* **2008**, *47*, 4861–4876.
- [43] a) H. Wang, W. T. Yang, Z. M. Sun, *Chem. Asian J.* **2013**, *8*, 982–989; b) G. Y. Wang, L. L. Yang, Y. Li, H. Song, W. J. Ruan, Z. Chang, X. H. Bu, *Dalton Trans.* **2013**, *42*, 12865–12868; c) D. Tian, R.-Y. Chen, Z. Chang, G.-Y. Wang, X.-H. Bu, *J. Mater. Chem. A* **2014**, *2*, 1465–1470; d) M. Guo, Z. M. Sun, *J. Mater. Chem.* **2012**, *22*, 15939–15946.
- [44] A. J. Lan, K. H. Li, H. H. Wu, D. H. Olson, T. J. Emge, W. Ki, M. Hong, J. Li, *Angew. Chem. Int. Ed.* **2009**, *48*, 2334–2338; *Angew. Chem.* **2009**, *121*, 2370–2374.
- [45] S. S. Nagarkar, B. Joarder, A. K. Chaudhari, S. Mukherjee, S. K. Ghosh, *Angew. Chem. Int. Ed.* **2013**, *52*, 2881–2885; *Angew. Chem.* **2013**, *125*, 2953–2957.
- [46] O. W. Webster, *J. Polym. Sci. Part A* **2002**, *40*, 210–221.
- [47] R. A. Sanchez, J. P. Ferris, L. E. Orgel, *Science* **1966**, *154*, 784–785.
- [48] H. Mizutani, M. Takahasi, H. Noda, *Origins Life* **1975**, *6*, 513–525.
- [49] J. Danielsson, M. Meuwly, *J. Phys. Chem. B* **2007**, *111*, 218–226.
- [50] a) Y. Wang, L. Cheng, Z.-Y. Liu, X.-G. Wang, B. Ding, L. Yin, B.-B. Zhou, M.-S. Li, J.-X. Wang, X.-J. Zhao, *Chem. Eur. J.* **2015**, *21*, 14171–14178; b) Y. Wang, X.-G. Wang, B. Yuan, C.-Y. Shao, Y.-Y. Chen, B.-B. Zhou, M.-S. Li, X.-M. An, P. Cheng, X.-J. Zhao, *Inorg. Chem.* **2015**, *54*, 4456–4465.
- [51] Y. Wang, J.-M. Yi, M.-Y. Zhang, P. Xu, X.-J. Zhao, *Chem. Commun.* **2016**, *52*, 3099–3102.
- [52] G. M. Sheldrick, SHELXS 97, *Program for the Solution of Crystal Structures*, University of Göttingen, Göttingen (Germany), **1997**.
- [53] G. M. Sheldrick, SHELXL 97, *Program for the Refinement of Crystal Structures*, University of Göttingen, Göttingen (Germany), **1997**.
- [54] J.-S. Hu, Y.-J. Shang, X.-Q. Yao, L. Qin, Y.-Z. Li, Z.-J. Guo, H.-G. Zheng, Z.-L. Xue, *Cryst. Growth Des.* **2010**, *10*, 4135–4142.

Received: January 16, 2016

Revised: April 16, 2016

Published online on ■ ■ ■ ■, 0000

FULL PAPER



Go for the quench: A bidentate ligand, 1-[4-[4-(1*H*-1,2,4-triazol-1-yl)phenoxy]-phenyl]-1*H*-1,2,4-triazole (TPPT), has been designed and synthesized (see scheme). By using TPPT as a building block for self-assembly with

Cd(NO₃)₂·4 H₂O and CdCl₂·10.5 H₂O, 1D double-chain and 2D (4,4)-layer compounds have been constructed. These complexes are used to detect Ca²⁺ and cyano complexes.

Self-Assembly

Y. Wang, P. Xu, Q. Xie, Q.-Q. Ma, Y.-H. Meng, Z.-W. Wang, S. Zhang,* X.-J. Zhao,* J. Chen,* Z.-L. Wang*



Cadmium(II)-Triazole Framework as a Luminescent Probe for Ca²⁺ and Cyano Complexes

